SPS Wideband Transverse Feedback Kicker: Design Report

J. M. Cesaratto, J. D. Fox, and C. H. Rivetta
Accelerator Research Department, SLAC National Accelerator Laboratory, 2575 Sand Hill Rd. Menlo Park, CA 94025

D. Alesini, A. Drago, A. Gallo, F. Marcellini, and M. Zobov
INFN-LNF, Via E. Fermi, 40 00044 Frascati (Roma), Italy

S. De Santis, Z. Paret, A. Ratti, and H. Qian
Lawrence Berkeley National Laboratory, 1 Cyclotron Rd. Berkeley, CA 94720

H. Bartosik, W. Hofle, and C. Zannini
CERN, Geneva, Switzerland

Abstract: The SPS wideband transverse feedback system is being developed to control vertical beam instabilities arising from intensity dependent effects like electron cloud instability (ECI) and the transverse mode coupling instability (TMCI). As part of the LHC Injector Upgrade (LIU) project, a wideband kicker is necessary as a damper to control unstable modes within a bunch. Several types of kicker structures, including cavities, striplines, and slotted structures have been studied to evaluate the operating bandwidth, transverse shunt impedance, and beam coupling impedance. Studies and results from all structures are described below, including three potential paths to implement these structures as a wideband kicker system. A single, slotted-coaxial kicker of 1 m length provides substantial kick strength (integrated transverse voltage) over a bandwidth ranging from nearly DC to 1 GHz. An array of four 10 cm long striplines provides substantial kick strength from DC to 750 MHz. For a given amplifier power of 500 W, the array of striplines can provide twice the transverse detecting voltage as the slotted kicker for frequencies up to 200 MHz. At frequencies 800 – 1000 MHz the transverse voltage generated by the slotted kicker dominates that of the stripline array. We recommend to CERN that both the slotted-coaxial kicker and the array of striplines should undergo more detailed mechanical design and be built as prototype wideband kickers for installation in the SPS.

SPS Wideband Transverse Feedback Kicker: Design Report

J. M. Cesaratto,* J. D. Fox, and C. H. Rivetta

Accelerator Research Department, SLAC National Accelerator Laboratory, 2575 Sand Hill Rd. Menlo Park, CA 94025

D. Alesini, A. Drago, A. Gallo, F. Marcellini, and M. Zobov

INFN-LNF, Via E. Fermi, 40 00044 Frascati (Roma), Italy

S. De Santis, Z. Paret, A. Ratti, and H. Qian

Lawrence Berkeley National Laboratory, 1 Cyclotron Rd. Berkeley, CA 94720

H. Bartosik, W. Hofle, and C. Zannini

CERN, Geneva, Switzerland

(Dated: September 9, 2013)

The SPS wideband transverse feedback system is being developed to control vertical beam instabilities arising from intensity dependent effects like electron cloud instability (ECI) and the transverse mode coupling instability (TMCI). As part of the LHC Injector Upgrade (LIU) project, a wideband kicker is necessary as a damper to control unstable modes within a bunch. Several types of kicker structures, including cavities, striplines, and slotted structures have been studied to evaluate the operating bandwidth, transverse shunt impedance, and beam coupling impedance. Studies and results from all structures are described below, including three potential paths to implement these structures as a wideband kicker system. A single, slotted-coaxial kicker of 1 m length provides substantial kick strength (integrated transverse voltage) over a bandwidth ranging from nearly DC to 1 GHz. An array of four 10 cm long striplines provides substantial kick strength from DC to 750 MHz. For a given amplifier power of 500 W, the array of striplines can provide twice the transverse deflecting voltage as the slotted kicker for frequencies up to 200 MHz. At frequencies $800 - 1000$ MHz the transverse voltage generated by the slotted kicker dominates that of the stripline array. We recommend to CERN that both the slotted-coaxial kicker and the array of striplines should undergo more detailed mechanical design and be built as prototype wideband kickers for installation in the SPS.

I. INTRODUCTION

Current plans for the HiLumi phase of LHC operation require an investment into upgrading the accelerators along the injector chain in the frame of the LHC Injector Upgrade (LIU) project [1–3]. This report concerns the last accelerator in the chain, the Super Proton Synchrotron (SPS). The purpose of this report is to establish a baseline for possible implementation of a transverse (vertical) kicker in conjunction with a wideband feedback system in the SPS to control beam intensity dependent instabilities caused by electron cloud (ECI) and transverse mode coupling (TMCI). The kicker (damper) structure is a critical component in this feedback loop, as it applies the wideband correction signal back onto the beam. The kicker options are evaluated via electromagnetic simulation considering the parameters of operating bandwidth, maximum transverse shunt impedance, and broadband beam coupling impedance. Additional aspects such as fabrication complexity, vacuum compatibility, and ease of coupling to external amplifier systems are also considered, but require more detailed mechanical design and consideration. From the information available, we have provided several solutions with frequency response up to 1 GHz. The required kick strength necessary has been estimated on the order of $10^{-5} - 10^{-4}$ eV$\cdot$s/m. The kicker must reside within the beam line vacuum system so the dimensions, aperture, and/or electrodes shall comply with all SPS stay clear limits and length limitations. The number of kickers or kicker signals and load ports is an important operational consideration, as every independent element that must be kept in precision timing with the beam adds operational complexity. This report explores three possible technical implementations of a kicker for the SPS transverse high bandwidth feedback system, and highlights the advantages and disadvantages of each.

A. Wideband Feedback Overview

The instability control problem requires technology to sense beam motion, compute a useful correction signal, and apply the correction signal back onto the particle beam. The beam physics determines the beam dynamics and issues of stability. The purpose of the feedback system is to change the beam dynamics to a stable case for all the operating parameters of the accelerator (energy, beam current, filling pattern, electron cloud density, HOM impedances, etc.). The feedback system must have sufficient bandwidth to sense and correct motion

---

* Electronic address: cesaratto@stanford.edu

within the individual bunches in order to correct the intra-bunch motion of ECI and TMCI. This is challenging for pickup and kicker structures, which must have useful bandwidths, and reasonable phase responses over roughly a gigahertz for the SPS cases. This large bandwidth is also challenging for the signal processing, which must have A/D and D/A functions with 2 – 8 GHz sampling rates, and support the computation of correction signals at these high throughputs. The basic formalism, which is in development at SLAC, can generate useful correction signals for both coupled-bunch and intra-bunch instabilities anticipated for the SPS through the HiLumi upgrade of the LHC.

B. Potential Kicker Structures

Three potential structures have been studied for use as kickers in the SPS. Stripline kickers have been used in the field for many years and have well established properties. They are attractive for their high shunt impedance at low frequencies, and they have DC response when used transversely. They can be tapered to provide continuous frequency response, but their ultimate band coverage and maximum shunt impedance are determined by their length. Generally speaking, shorter striplines will extend to higher bandwidth, but will have lower shunt impedance. They can be used in arrays to increase the shunt impedance with appropriate delay and synchronization between multiple striplines.

Cavity kickers are attractive for their high shunt impedance, although they are relatively narrowband. However, by damping the cavity, the Q can be reduced, thereby increasing the bandwidth. Depending on the geometrical design of the cavity the band of coverage can be adjusted. Multiple bands of cavities would be necessary to cover the full band necessary, which could lead to complexity in the signal processing, phasing, and equalization.

Slotted or slotline kickers similar to those used in the CERN ISR and $\bar{p}$-complex [4] and Fermilab $\bar{p}$-Accumulator [5] for stochastic cooling are also considered. These structures couple power from waveguides or transmission lines to the beam pipe via small periodic slots. These structures can be tuned dimensionally to provide the necessary bandwidth and shunt impedance. Like any of these structures, installation into the machine will contribute to the beam coupling impedance of the machine. Since these structures have many small periodic slots they must be studied carefully for the beam

impedance impact.

Evaluation and analysis of each of these structures are provided in this design report for their operational bandwidth, transverse shunt impedance, and in two cases, beam coupling impedance. Operational use and fabrication complexities will be evaluated for all designs. Each must comply with the existing SPS restrictions and constraints. The report will include three potential paths for fabrication weighing the advantages and disadvantages of each. Finally, the report will conclude with a recommendation with respect to the three proposed paths for detailed development and design of a vacuum compatible prototype for beam tests in the SPS after Long Shutdown 1 (LS1).

C. Existing SPS Parameters and Constraints

1. Installation Location

Figure 1 shows a schematic view of the layout of the SPS (see Ref. [6] for a scaled version with transfer lines shown). The proposed location for the new wideband kicker will be in Long Straight Section 3 (LSS3) of Sextant 3 in the SPS. This region marks the start of the arc in the dispersion suppressor region of the machine, containing flat vacuum chambers. The ∼13 m long location where the kickers will be installed is shown in Fig. 2. Because of beam aperature (stay-clear) requirements, only about 8 m of the space is usable (see Sect. I C 2). LSS3 is a low radiation area of the SPS with existing RF infrastructure. Cabling and preparation of the space has begun as a part of LS1 work. Preparing the space will include reshuffling equipment in LSS3 and installing a dummy chamber if the new kicker is not installed by the time the SPS becomes operational again at the end of LS1. As an alternative location, LSS5 has also been considered, but it does not have existing RF infrastructure. In LSS5 an experimental chamber would be available to install auxiliary equipment such as power amplifiers.

2. Beam Aperture

Beam aperture studies have been performed by CERN's ABP group in order to estimate the transverse beam stay clear region for the new kicker. The aperture can be estimated by the following expression

$$a_x(s) = \frac{A_x(s) - \left[x_{\text{co}}(s) + \Delta_{\text{co}}\sqrt{\beta_x(s)/\hat{\beta}_x} + (1 + k_\beta)\left(|D_x(s)| + k_{D_x}\hat{D}_x\sqrt{\beta x(s)/\hat{\beta}_x}\right)\hat{\delta}\right]}{(1 + k_\beta)\sqrt{\beta_x(s)\epsilon_x}} \tag{1}$$

where a_x is the available aperture (normalized to the RMS beam size) for direction x, A_x is the physical aperture, x_{co} is the closed orbit, Δ_{co} is the maximal closed
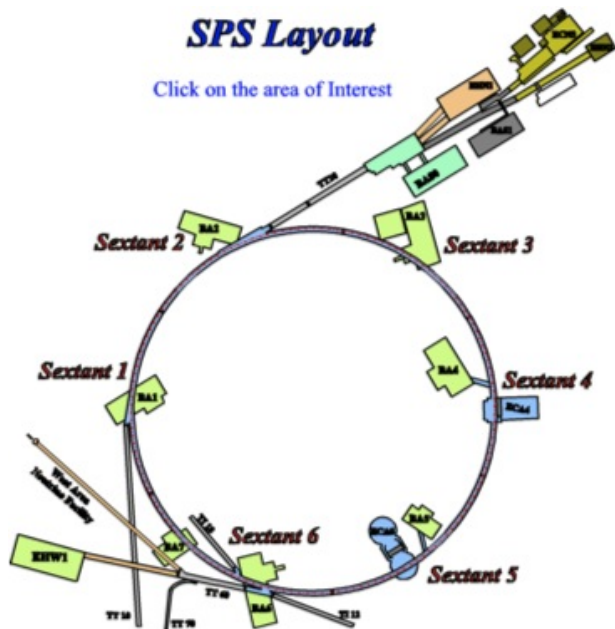
FIG. 1. Layout of the SPS. The proposed location for installation of the new wideband kicker will be in LSS3 of Sextant 3. LSS5 is also considered as an alternative location for installation.
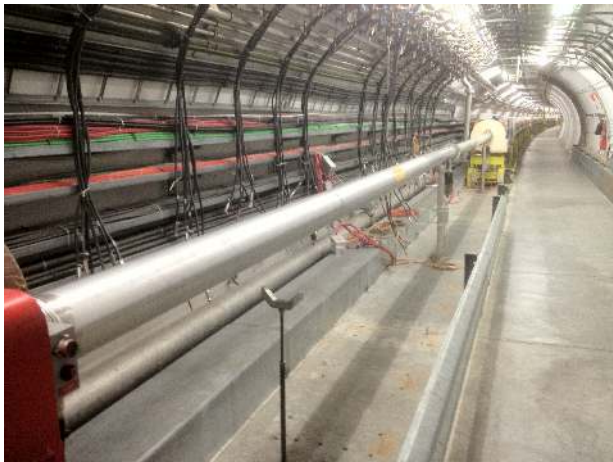

FIG. 2. Precise location in LSS3 of the SPS where the new kicker system will be installed. About 13 m of longitudinal space is available, but only about 8 m of that space is usable because of beam aperture (stay-clear) considerations.

orbit distortion, β_x is the beta function, $\hat{\beta}_x$ is the peak beta function, D_x is the dispersion, $\hat{D}_x$ is the peak dispersion, k_β is the beta beat factor, k_{D_x} is the dispersion beat factor, ϵ_x is the physical emittance, and $\hat{\delta}$ is the peak momentum spread. Following a conservative approach, estimates were calculated to stay in the shadow of the local aperture restrictions. In the horizontal plane, there are two choices, as shown in Fig. 3. The first, in blue, rep-

resents a linear interpolation between QF and the MBB dipole aperture to stay completely in the shadow whereas the second, in red, shows the aperture required for the CNGS beam with Q20 optics[1]. In the vertical plane, the aperture half width is constant at 20 mm, which is just slightly larger than the MBA vacuum chamber height of 39.3 mm. Horizontally, the aperture half width is smaller at MBB.32150 at 55 mm. As one moves away from dipole magnet, the aperture increases and at 8 m downstream the aperture half width is 66 mm. Thus, the new kickers will have an aperture that must be larger then 40 mm in the vertical direction and 132 mm in the horizontal direction.
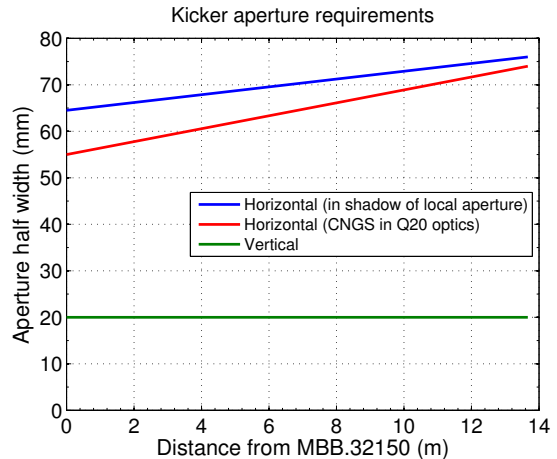

FIG. 3. Calculated aperture requirement for the kicker within the installation region of LSS3.

3. SPS Operating Modes

The RF frequency of the SPS is 200 MHz, with a small component at the 4th harmonic at 800 MHz added by dedicated cavities. The 200 MHz RF system defines an RF bucket width of $\sim$5 ns length and harmonic number of 4620. The typical bunch length is represent as $4\sigma_z$ of a normal distribution, where $\sigma_z \simeq 0.7$ ns at injection energy (26 GeV). The bunch length becomes shorter during acceleration to flat top (450 GeV) where $\sigma_z \simeq 0.4$ ns.

Up to now, the operational LHC beam had a bunch separation of 50 ns. The bunch intensity for typical 50 ns spaced beam was 1.7×10^{11} p ($\epsilon_{x,y}^{rms} = 1.7$ μm) and because of higher bunch intensity and lower emittance,

---

[1] The Q20 optics are not presently used for the high intensity CNGS beam but could be considered for operation with high intensity fixed target beams in the future. Since the Q20 optics has higher beta functions and dispersion function compared to the SPS design optics (Q26), the aperture calculations presented here were performed with the Q20 optics.

the high energy physics experiments experienced pile-up. Thus, to reduce pile-up at increased luminosity, the goal is to run at 25 ns bunch spacing. Table I contains a listing of the bunch intensity, emittance, and bunch length at 450 GeV for present and future LHC beams.

The filling scheme for LHC beams, populates every fifth bucket, leaving a 25 ns bunch spacing or a bunch repetition rate of 40 MHz. Typically, each full batch consists of 72 bunches, with at most 4 batches accelerated in a single SPS ramp cycle, each batch separated by 45 buckets. Thus, up to 288 bunches may be present in the machine[2]. The typical bunch intensity today for 25 ns spaced beams is 1.2×10^{11} p at extraction. Notice that HL-LHC beams call for nearly twice the bunch intensities of today, and the kickers and loads must be able to handle such beam induced power.

One disadvantage of using 25 ns beams is evidence of Ecloud effects, which include vacuum pressure rise, transverse instabilities, losses, and emittance blow-up. As a method to mitigate electron cloud, scrubbing runs have been performed over the years with 25 ns spaced beams. Recently, a doublet scrubbing beam has been studied and shows high scrubbing efficiency [7]. This type of beam contains 25 ns spaced bunch doublets, with the doublets spaced at 5 ns.

TABLE I. Present and future LHC beam parameters for standard production injection fills (beam energy 450 GeV) [8]. B_l is the $4\sigma_z$ bunch length.

		N ($10^{11}p/b$)	$\epsilon_{x,y}^{rms}$(μm)	ϵ_z (eVs)	B_l (ns)
Achieved	50 ns	1.70	1.71	0.5	1.65
	25 ns	1.20	2.60	0.45	1.55
LIU	25 ns	2.00	2.08	0.45	1.55
HL-LHC	50 ns	3.68	2.50	0.5	1.65
	25 ns	2.32	2.08	0.45	1.55

4. Existing SPS Feedback

The existing SPS vertical feedback operates with two kicker deflectors kicking with the electric field only, installed at a $\beta = 42$ m in point 2 of the SPS [9]. Each kicker has a length of 1536 mm, and is operated by a power amplifier with two 30 kW tetrodes in push-pull configuration developing a maximum of 2.6 kV over the gap of 38 mm. The combined transverse kick voltage for low order coupled bunch modes is 215 kV corresponding to 7.2×10^{-4} eV·s/m and can damp injection errors on the order of several millimeters within 20 turns. At 20 MHz,

the maximum operating frequency, the kick strength is reduced to 1.58×10^{-4} eV·s/m.

At first glance, it appears that the new transverse damper must reach as low as 40 MHz (the bunch repetition frequency for LHC beams), in order to kick every bunch of the 25 ns spacing regime. But, the new scrubbing beam presents a situation where a bandwidth of 20 – 100 MHz would be necessary with the 5 ns doublet spacing to cover all possible coupled bunch modes. If the two bunchlets oscillate out of phase, there is currently no system to correct this, so there is a desire that the new wideband damper overlap in frequency with the existing transverse damper at the low frequency end.

5. Transverse Beam Offset

The kicker structure must be able to provide a reasonably uniform kick over the region in vacuum space that the beam may reside. Initially, we have been provided estimates of a worst case scenario, a 5 ns beam with the Q20 optics and 3.5 μm transverse emittances. Vertically, the good field region should be ±15 mm from the axis. Horizontally, it depends on how close the kicker is installed to the MBB dipole, but for a 1 m long kicker, ± 25 mm from axis may be sufficient. Considering the entire available space the requirement is ±40 mm.

6. SPS Transverse Impedance Budget

The effective beam impedance [10] of the new wideband kicker should be compared with the effective impedance of the installed devices. The total measured effective vertical impedance of the SPS is around 18 MΩ/m [11]. Based on 3D simulations, coaxial wire measurements, beam-induced heating measurements and history of the measured effective vertical impedance, the kickers are the most important contributors (around 7 MΩ/m) [11]. Presently, there are 19 kickers installed in the machine, with an average contribution per kicker of ∼0.37 MΩ/m. The beam coupling impedance of the new wideband kicker should not exhibit narrow resonances and must contribute less than the average impedance per kicker. Preferably, the beam coupling impedance should not exceed about 1% of the total SPS impedance, i.e., ∼0.18 MΩ/m.

7. Existing Tapered Stripline Operated as a Kicker

The existing kicker currently in use at the SPS for the wideband feedback development effort is a tapered exponential stripline pickup, developed in the 1970's for beam instrumentation purposes, and installed backwards for historical reasons [12]. The stripline consists of four electrodes exponentially tapered in width and in distance

---

[2] For purposes of non-LHC beam e.g., scrubbing beams, more batches may be injected with higher repetition frequency, but at reduced bunch intensities

from the vacuum chamber wall to maintain a $50\,\Omega$ characteristic impedance. When used as a kicker, the frequency response rolls off at $f_0 = 158$ MHz. For the feedback demonstration experimental setup, with a 100 W amplifier powering each electrode, a momentum change, $\Delta p_\perp = 4\times10^{-6}$ eV·s/m is generated (empirically determined) corresponding to a transverse deflecting voltage of $V_\perp^{\rm DC} = 1.2$ kV at DC. Folding in the frequency response, the transverse voltage on axis is shown in Fig. 4 and represented as

$$V_\perp = \frac{V_\perp^{\rm DC}}{1 + \frac{i\omega}{(\beta va/2L)}} \left[1 - e^{-a}e^{-i\omega L/\beta v}\right] \qquad (2)$$

where v is the velocity of the beam, $a = 2.485$ is the attenuation constant of the taper, and L is the 0.375 m electrode length [12]. It is clear that a structure is needed, which will extend to higher frequency and still provide sufficient kick strength. As a guideline (still very much under study), we desire a momentum change greater by about an order of magnitude, 5×10^{-5} eV·s/m over the present stripline's performance. We will use the transverse voltage of the existing exponentially tapered stripline as a baseline for comparison to the new kicker designs.
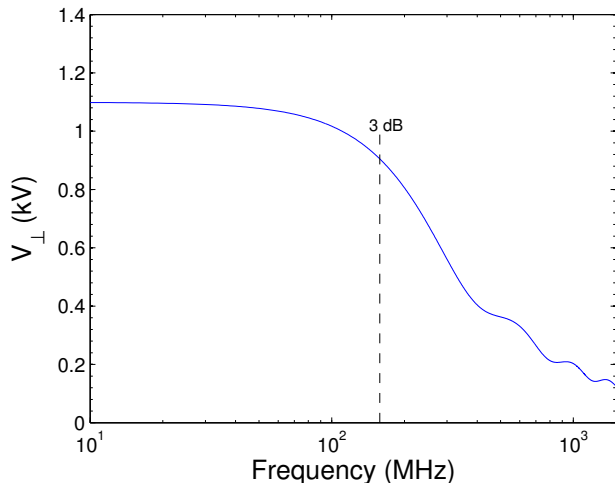

FIG. 4. Transverse deflecting voltage generated on axis by the existing exponentially tapered stripline powered by four 100 W amplifiers. The 3 dB roll-off point at 158 MHz is indicated by the vertical dashed line.

II. KICKER DESIGN CRITERIA AND EVALUATION

The structures were evaluated with respect to their characteristics of bandwidth, transverse shunt impedance, and beam coupling impedance via electromagnetic simulations. The parameters of each structure were tailored in simulation to be consistent with the SPS constraints and system requirements.

A. Bandwidth

The operating bandwidth is required to be very large to provide bunch to bunch kicks as well as intra-bunch kicks. The modes that drive the bunch unstable are still under study, so a requirement on the upper frequency needed is still being refined, but at this time a goal of 1 GHz has been set. A lower frequency bound of 10 MHz seems necessary to overlap with the existing transverse damper for the scenario of beam scrubbing, as described in Sec. I C.

B. Transverse Shunt Impedance

The transverse shunt impedance, $R_\perp T^2$, of a kicker relates the ratio of the square of the structure's voltage to twice the total input power $P_{\rm tot}$, according to [13]

$$R_\perp T^2 = \frac{V_\perp^2}{2P_{\rm tot}} \qquad (3)$$

where T is the transit-time factor, representing the reduction in integrated kick by not experiencing the maximum field everywhere within the kicker. $V_\perp$ is the transverse voltage and is defined as

$$V_\perp(\hat{x}, \hat{y}) = \int_0^L \left(\mathbf{E} + \mathbf{v} \times \mathbf{B}\right)_\perp dz. \qquad (4)$$

Equation 4 in our case can be simplified as

$$V_\perp = V_\perp(\hat{y}) = \left| \int_0^L \left[E_y(z) + cB_x(z)\right] e^{\frac{j\omega z}{\beta c}} dz \right| \qquad (5)$$

where the beam propagates in the z-direction, $E_y(z)$ and $B_x(z)$ are complex fields in the vertical and horizontal directions, respectively, $e^{\frac{j\omega z}{\beta c}}$ accounts for the beam transit time and has positive argument if the electromagnetic field co-propagates with the beam and negative argument if the field counter propagates with the beam, and L is the length of the structure. This resulting voltage yields the maximum vertical kick of the structure, which when used in conjunction with Eq. 3 shows that for maximum transverse voltage or kick strength, the shunt impedance must be maximized.

C. Beam Coupling Impedance

As a charged beam moves through an accelerator, it will induce electromagnetic fields within the surrounding conducting vacuum pipe, which can affect the dynamics of the beam. Analysis in the time domain yields these

fields, known as wake fields. The wake potential is the momentum change of the beam from the induced fields. The wake function is the wake potential normalized to charge, has units of V/C, and can be expressed longitudinally by $W_{||}^m(z)$ and transversely by $W_{\perp}^m(z)$, where m is the moment of the wake function. In the frequency domain, the Fourier transformation of the wake function yields the beam coupling impedance, longitudinally, in units of Ω and transversely in units of Ω/m for the first and second order impedances, respectively. The longitudinal and transverse coupling impedances can be represented respectively as

$$Z_{||}(\omega) = \frac{1}{\beta c}\int_{-\infty}^{\infty} W_{||}(z)e^{\frac{-j\omega z}{\beta c}}\, dz \qquad (6)$$

$$Z_{\perp}(\omega) = \frac{j}{\beta c}\int_{-\infty}^{\infty} W_{\perp}(z)e^{\frac{-j\omega z}{\beta c}}\, dz \qquad (7)$$

D. Electromagnetic Codes

The electromagnetic calculations for the evaluation of the structures were carried out numerically using codes ACE3P [14], GdFidL [15], HFSS [16], and CST [17]. GdFidL and CST are time domain based codes while HFSS is a frequency domain based code. ACE3P contains a suite of codes computing in both the time and frequency domain.

III. DISCUSSION

The three structures explored in this study each have advantages and disadvantages with regard to the characteristics necessary for the feedback system. In this section we evaluate three possible implementations of these structures since covering such a large bandwidth with sufficient shunt impedance is a tall task for a single structure. The three possible paths for implementation examined are 1.) a stripline with two narrowband cavities, 2.) an array of striplines, and 3.) a slotted-coaxial kicker. Additional details on the properties of each structure alone are included in the Appendix for further reference.

We would like to explain our nomenclature for power as it relates to the transverse voltage estimates. We will denote power in terms of the total power delivered to a kicker system, P_{tot}, as is used in Eq. 3. The power per amplifier is also used and will be represented as, P_{amp}. For a single stripline with two electrodes, two out of phase amplifiers are used and the total power becomes $P_{\text{tot}} = 2 \times P_{\text{amp}}$. For a single slotline the situation is similar, and for a single cavity typically one narrowband amplifier is used so $P_{\text{tot}}^{\text{cav}} = P_{\text{amp}}^{\text{cav}}$.

A. Stripline and Two Cavities

Cavities are rather narrowband structures, so to broaden the frequency coverage we suggest to use several cavities at multiples of a fundamental angular frequency, $\omega_0 = 2\pi/\tau_b$, where $\tau_b = 2.5$ ns (estimate at 26 GeV) is the bunch length $(\sim 4\sigma_z)^3$. Since low frequency cavities tend to be large in size, a stripline kicker with frequency response from DC to the fundamental frequency will be used in addition to the cavities.

As an example implementation we propose to use a stripline kicker covering the range from DC – 400 MHz, and two transverse cavities centered at the second and third harmonics with bandwidths on the order of the bunch repetition frequency, $f_b = 40$ MHz. A preliminary estimate of transverse shunt impedances of cavity kickers can be extrapolated by scaling results reported in the literature. The stripline has a length of $L = 0.17$ m and an electrode separation of $h = 0.045$ m, to comply with the stay-clear requirement. The proposed system is summarized in Tab. II. Assuming that each kicker listed

TABLE II. Proposed stripline-cavity system as an intra bunch kicker. The values here are scaled results from the literature.

Type	Stripline	Cavity #1[a]	Cavity #2[a]
Bandwidth (MHz)	DC - 400	800(16)	1200(16)
Length (cm)	17	15	10
Filling time (ns)	0.6	10	10
Q_L	-	25	38
Shunt Impedance (kΩ)	5.7 at DC	1.5	2.2

[a] The cavities operate with TM_{110} deflecting mode.

in Tab. II is powered by a 1 kW source covering the entire bandwidth, the resulting transverse voltage transferred to the beam as a function of frequency is shown in Fig. 5. Simulations of the cavities verify that the desired parameters listed in Tab. II are feasible (see Sec. A 2).

An attractive feature of this type of scheme is that very wideband kicker(s) and amplifier(s) are not necessary. However, this scheme would require N narrowband kickers and amplifiers to provide the overall required system bandwidth. The N narrowband kickers must then be timed and phased properly. The drive signal to the amplifiers requires N channel outputs from the processing of N frequencies. The input sequence requires DFT or FFT decomposition to identify each frequency, which are computationally intensive procedures. In addition, the output signals for each cavity would be played out at a different rate than the input signal at 40 MHz. For

---

[3] Note that this only an example. The bunch length is assumed to be fixed in this case, which is not the case for operational beams. When the beam length changes, the frequencies needed to kick will also change.
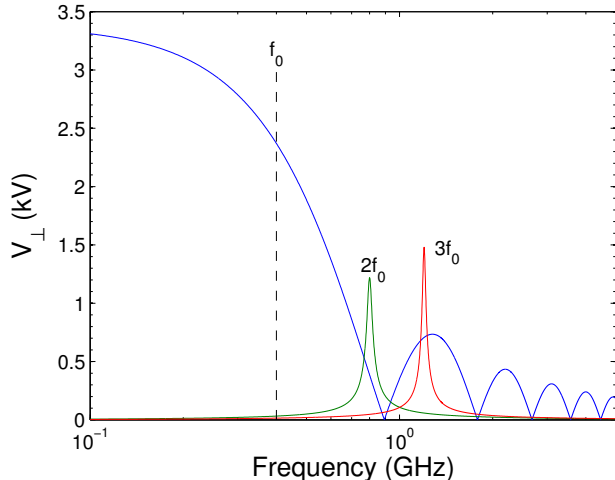
FIG. 5. Transverse deflecting voltages on the beam as a function of frequency for the stripline-cavity system assuming 1 kW power over the entire frequency span. f_0 indicates the 3 dB roll-off point for the stripline at 400 MHz, and $2f_0$ and $3f_0$ indicate the two cavities' operating frequencies.

LHC type beams, the 25 ns between bunches would be needed to fill the cavity kickers. With the doublet scrubbing beam this would not be possible since the spacing is 5 ns and the filling times for the cavities are 10 ns.

The processing involved for this type of modal system is intensive and does not follow the present time-domain, single output channel approach that has been undertaken with the feedback demonstration system to date. We feel that although this is a very interesting approach, considering the processing hardware developed so far, and the complexity of synchronizing multiple kickers, that having a single channel system over the entire band is a very desirable feature. With that in mind, we suggest two more solutions, which are in tune with the present processing architecture.

B. Array of 10 cm Striplines

A stripline shorter than the one mentioned in Sec. III A has a frequency response that extends across the entire feedback bandwidth, without recourse to cavity kickers. The drawback is reduced shunt impedance, which scales with the square of the length, L, so that multiple kicker modules have to be used in order to keep the power per stripline down to a manageable level. This solution offers the advantage of being able to reach the desired momentum kick by simply increasing the number of kicker modules, while maintaining the amplifier power at a convenient level. On the other hand, a compromise between the number of modules N_k and total space occupied by the kicker system is the main limiting factor.

Since the number of modules scales with the inverse of

the square root of the amplifier power, and amplifier cost scales at least linearly with the amplifier power, it can be shown that as long as the cost of a single amplifier is comparable with the cost of a stripline module (which is true except than for rather low powers), then the solution with lower power amplifiers and more modules is the cost effective one. Using a 10 cm long stripline optimizes the impedance at 750 MHz, while still supplying a 1.8 kΩ shunt impedance at low frequency for each kicker module and in our judgment this appears to be the best solution for the stripline length, balancing required power and number of kicker modules as shown in Eq. 8 derived for a SPS vertical stay-clear of 45 mm:

$$N_k = \frac{\frac{\Delta p}{e}c}{2\sqrt{R_\perp T^2 P_{\text{tot}}}} \approx \frac{1}{8.4}\frac{\frac{\Delta p}{e}c}{L_{(cm)}^{\text{eff}}\sqrt{P_{\text{tot}}}} \qquad (8)$$

where

$$L_{(cm)}^{\text{eff}} = L\frac{\sin(\omega L/c)}{\omega L/c} \qquad (9)$$

is the stripline physical length, expressed in centimeters, corrected by an impedance roll-off factor, which is equal to 1 at DC and goes down to about 0.5 at 1 GHz.

Figure 6 shows the integrated transverse deflecting voltage for a four module kicker, where each module is driven by two 500 W maximum power amplifiers, in green, and by two 100 W, in red. Such a number of modules can be installed in a less than 1 m long portion of beam pipe and therefore provides a direct comparison with the 1m long slotted-coaxial structure described in Sec. III C and particularly Fig. 7. It is worth pointing out that this stripline array makes use of eight amplifiers, whereas the slotted structure uses two amplifiers. Compared with the existing tapered stripline using 100 W amplifiers, the array of striplines supersedes in integrated transverse voltage over the entire frequency span. At low frequency the voltage is a factor of 3.5 larger while at 1 GHz provides 1.5 kV deflecting voltage.

From Fig. 6 we can see that the voltage provided at lower frequencies is about one half of the voltage required to achieve 5×10^{-5} eV·s/m (15 kV) transverse momentum kick using two 500 W amplifiers. From Eq. 8 we can see that in order to provide the entire kick strength at low frequencies, either the number of elements N_k has to be doubled, thus increasing the overall length to over 2 m, or the amplifier power has to be increased four-fold, or a combination of the two.

If we look at the high frequency end of the stripline array response, we see that an additional factor of two would be necessary to reach the nominal momentum kick at 1 GHz. Again, one has to consider what the actual required kick is and how practical it would be to increase the number of elements and/or the amplifier power. One could also consider splitting the bandwidth into a lower-power amplifier up to $500 - 600$ MHz and a higher-power amplifier for the frequencies up to 1 GHz.

As opposed to the stripline and two cavity scenario, no special synchronization is required in this case, since it is
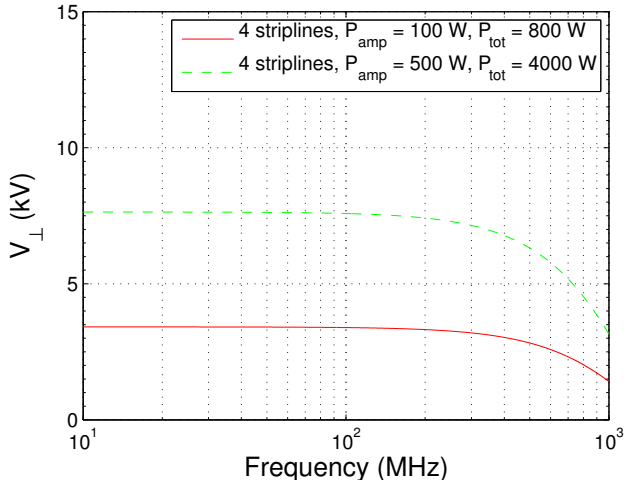
FIG. 6. Total transverse deflecting voltage for a four module 10 cm long stripline kicker, assuming that each module is driven by two 100 or 500 W power amplifiers over the entire frequency span.

sufficient to introduce a fixed delay between the stripline modules to phase them appropriately, which would be of the order of 1 ns. Similar to the number of amplifiers, eight loads are also necessary to dissipate beam induced power on the upstream port.

Another multiple stripline strategy might be to use several stripline lengths in the array, with several high frequency short striplines in conjunction with a smaller number of longer low-frequency driver elements. This still requires multiple amplifiers (or a multi-output high power splitter system). For multiple amplifiers, they may be differing in bandwidth depending on with which length driver element they are paired. This approach may be economically better to achieve the total integrated kick voltage, though it adds complexity in the numbers of types of amplifiers required to maintain and may be unattractive in operation considering operational spare requirements.

C. Slotted-Coaxial Structure

Of the three types of slotted kickers explored, the slotted-coaxial kicker option is very attractive for several reasons. Foremost, it has frequency response from nearly DC up to 1 GHz for a structure of 1 m length as seen by the black curve in Fig. 24. The shunt impedance at low frequency is 5 kΩ and at 1 GHz is 11 kΩ. Across that entire frequency range, a shunt impedance of at least >5 kΩ is maintained. Thus, this one structure has the capability to operate over the full bandwidth. In effect, this would minimize the number of vacuum structures, feed throughs, amplifiers, and associated hardware necessary. Another very attractive feature of the slotted-

coaxial kicker is that the voltage transferred to the beam is nearly phase linear over the operating band as can be seen in Fig. 23. Only at high frequencies near 1 GHz, does the phase response deviate from linearity. This is an important consideration contributing to the phasing and overall transfer function of the feedback system. Parameters of the optimized slotted-coaxial kicker are listed in Tab. III. The transverse deflecting voltage generated on the beam as a function of frequency of the slotted-coaxial kicker is shown in Fig. 7 for several total input powers. Using two existing 100 W amplifiers out of phase on each electrode suppling a total of 200 W, the transverse voltage on axis is 25% higher than the existing tapered stripline at frequencies below 100 MHz, and covers the entire frequency band up to 1 GHz. By using 1 kW of power total power (500 W per electrode), the transverse voltage on axis is increased by a factor 3.2 at low frequencies over the existing stripline and much more at high frequencies. By using 4 kW of total power, the transverse voltage is 6.7 kV, just under half of the desired voltage for frequencies below 500 MHz, but increases slightly to 9.5 kV at 1 GHz. As stated before, the desired transverse voltage or kick strength is still under scrutiny.

The slotted-coaxial kicker as modeled honors the stay-clear with room to spare. If more transverse voltage is needed, the height of the beam piper can be reduced from the modeled 52.3 mm to 45 mm (or even 40 mm), still abiding by the stay-clear requirements. Simulations show that for a 45 mm beam pipe height the shunt impedance would be boosted by about 20% across the entire frequency range. This corresponds to an increase in transverse voltage of 4.5%.

TABLE III. Dimension parameters of the slotted-coaxial after optimization for bandwidth and shunt impedance. These parameters correspond to those used to calculate the transverse deflecting voltage in Fig. 7 and the shunt impedance (black curve) of Fig. 24. See Fig. 21 for a diagram of dimensions.

Parameter	Description	Dimension (mm)
al	Length of slotted section	1000
bh	Beam pipe height	52.3
bw	Beam pipe width	132
thick	Slot interface thickness	1
wh	Waveguide height	50
ww	Waveguide width	150
ss	Slot spacing	12.5
sl	Slot length	80
sw	Slot width	12.5
L	Length vacuum pipe at ends	200
h_inner	Coaxial line thickness	5
w_inner	Coaxial line width	80

One of the major concerns for this type of structure is its contribution to the impedance of the machine. Initial evaluations show that this structure does not exceed 0.18 MΩ/m or 1% of the total SPS impedance. However, the slotted kicker impedance must still be added to the
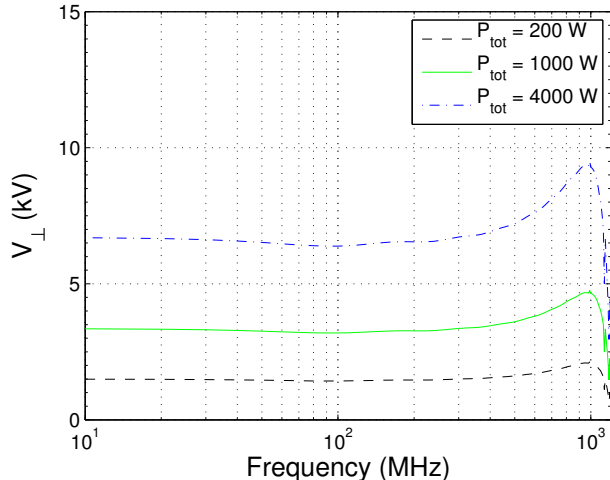
FIG. 7. Transverse deflecting voltages on the beam as a function of frequency for the slotted-coaxial kicker for total input powers of 200 W (black, dash), 1000 W (green, solid), and 4000 W (blue, dash-dot) for the parameters listed in Tab. III.

impedance model of the SPS as a final determinant of whether this structure will comply with the requirement. Beam coupling impedance calculations are included in App. C 4.

Since the design has been on a strictly electromagnetic basis, more detailed mechanical design is necessary. For instance, feed throughs need to be designed. In addition, the over 1 m long strip in the waveguide must be supported, most likely be means of dielectric materials in vacuum, which can affect the electromagnetic properties of the structure. Additionally, heat load and mechanical stress calculations are necessary before construction can begin.

A practical (and operational) aspect of any of these structures is the management of beam induced power, and the requirement to protect the amplifier systems from beam induced power. These requirements have not been studied in detail, though the in-band directivity of the striplines is helpful, and the cavity systems have no directivity but may be paired with a finite bandwidth circulator to protect the amplifier. The slotline beam induced power management requires more study.

D. Array of Striplines vs. Slotted-Coaxial Structure

The two options that seem most feasible with the current processing formalism are the array of four 10 cm striplines and the 1 m long slotted-coaxial structure. To visually compare the transverse voltages between the two, they have been overlaid on the same plot in Fig. 8. For a similar amount of total amplifier power, $P_{tot} = 4$ kW, the integrated deflecting voltage of the stripline ar-

ray is about 12% larger than the slotted structure at low frequencies. At 350 MHz, the voltages are equal (7 kV), as the stripline voltage decreases for high frequencies and the slotted kicker voltage increases for high frequencies. In the stripline case, since we have four modules, with two electrodes per module, the amount of power per electrode (or amplifier) is $P_{amp} = 500$ W. The slotted kicker requires two amplifiers at 2 kW each. Even though the total number of amplifiers in the stripline case would be more at lower power, broadband 500 W amplifiers have advantages over broadband 2 kW in cost and size. Above about 1 kW the size of these amplifiers are large (cabinet-sized), and thus, if they are stored in the SPS tunnel, will need to be properly stored and shielded. Lower power amplifiers are characteristically more reliable, easier to replace, and less costly per each unit.

A more useful comparison is to use a given amplifier power per unit instead of comparing each structure supplied with the same total power. For example, if P_{amp} = 500 W, the array of four striplines, the total power remains the same at 4 kW. However, for the slotted kicker case with 500 W amplifiers, the total power is 1 kW. The transverse voltage for the stripline case is a factor of two higher than the slotted case at frequencies up to 200 MHz. The transverse voltage between the kickers is equal at 4.5 kV at 800 MHz, as the stripline voltage decreases and the slotted voltage increases for higher frequencies. This analysis shows, that for frequencies below about 750 MHz, the stripline array is advantageous, but above 750 MHz, the slotted kicker is superior.
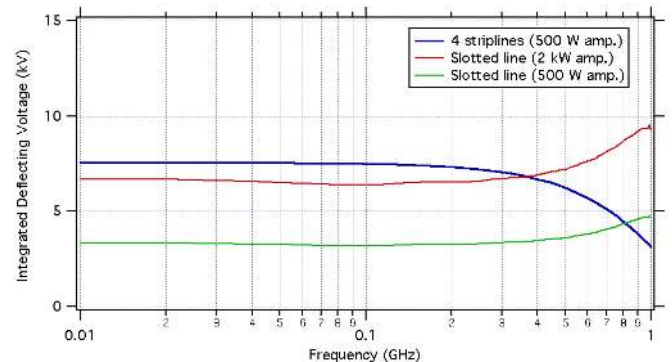

FIG. 8. Transverse voltage of the stripline and slotted-coaxial kickers for particular amplifier powers. The powers listed in the legend are per amplifier, P_{amp}.

If the entire usable space available in the SPS was filled with kickers (and beam impedance not considered), which is about 8 m, we could accommodate about 44, 10 cm striplines and six, 1 m slotted kickers. For the array of 44 striplines, to maintain at least 15 kV across the entire frequency band, each electrode must be powered by a 100 W wideband amplifier. The number of amplifiers needed would be 88 and the total power to the array is 8.8 kW. The transverse voltage at 100 MHz is 38 kV, much higher than the desired voltage. However, the

TABLE IV. The integrated transverse voltage as a function of frequency (for a given number of kicker modules, amplifiers, and amplifier powers) for an array striplines and slotted-coaxial kickers (slotlines). The voltages for the stripline are based on theoretical calculations, which are systematically 20% higher at DC and 40% higher at 1 GHz than the simulation results. The voltages for the slotline are based of HFSS simulation results.

	N_{mod}	N_{amp}	P_{amp} (W)	P_{tot} (W)	$V_\perp$ (kV)				
					100 MHz	250 MHz	500 MHz	750 MHz	1000 MHz
Striplines	4	8	500	4000	7.6	7.3	6.3	4.9	3.2
Striplines	44	88	100	8800	37.3	35.9	31.1	23.9	15.5
Slotline	1	2	500	1000	3.2	3.3	3.6	4.2	4.6
Slotline	1	2	2000	4000	6.4	6.6	7.2	8.4	9.3
Slotline	6	12	300	3600	14.8	15.3	16.7	19.4	21.5

voltage drops drastically at 1 GHz to 15 kV. To reiterate, if the bandwidth necessary is reduced, many less amplifiers, amplifiers of less power, or less striplines would be needed. In the six slotted structures case, 12, 300 W wideband amplifiers would be needed to power each electrode for a total of 3.6 kW. The low frequency voltage is 15 kV at 100 MHz and increases to 22 kV at 1 GHz. This example drives home the point that if the bandwidth needed is less than about 750 MHz, the stripline array is the right choice, but if high frequency up to 1 GHz is needed, then the slotline is necessary.
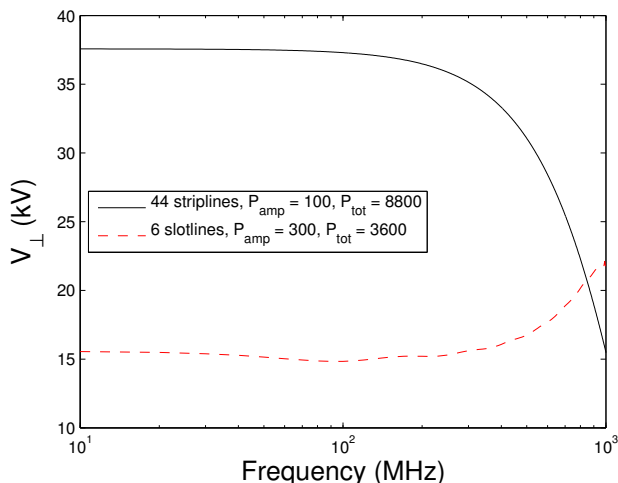
FIG. 9. Transverse voltage of the stripline array with 44, 10 cm long modules and the slotline with six, 1 m long modules. To maintain the desired transverse voltage of 15 kV across the entire 1 GHz operating band, 88, 100 W (P_{tot} = 8.8 kW) amplifiers are necessary for the stripline array, and 12, 300 W (P_{tot} = 3.6 kW) amplifiers are necessary.

E. Recommended Path for Fabrication

Table V summarizes the number of feed throughs, loads, and amplifiers needed for each kicker system. The stripline and two cavity approach requires three vacuum structures, one for the stripline and two for the cavities. The 0.17 m long stripline needs four feed throughs, two of which will be used for coupling high power to loads and two used for the drive signals. Thus two amplifiers are required, of 500 W in the band of near DC to 400 MHz. For each cavity, at least two feed throughs and two loads are needed. The presence of high order modes may require additional couplers and loads. Each cavity will be powered by a 1 kW amplifier, one in the band of 800 MHz and the other at 1200 MHz. The total power of this system would be 3 kW. For the array of four 10 cm long striplines, a 1 m long vacuum structure is needed to contain the four striplines. The vacuum structure will 16 couplers, 8 of which will be used for coupling high power to loads and 8 used for the drive signals. Eight 500 W amplifiers are needed in the band from nearly DC to 1000 MHz for a total power of 4 kW. For the slotted-coaxial kicker, one 1.4 m long vacuum structure is needed, with four couplers, two high power loads, and either two 500 W or two 2 kW, DC to 1000 MHz amplifiers, depending on what is commercially available and cost effective.

Of the three kicker systems presented, we recommend that both the array of four 10 cm long striplines and the 1 m long slotted-coaxial kicker undergo more detailed mechanical design and prototyping as wideband kicker system. The striplines have a clear advantage at frequencies below 750 MHz whereas the slotline has the advantage above 750 MHz extending to 1000 MHz. In discussions with the CERN RF group, we find it advantageous to pursue both alternatives. For minimal additional cost and lead time, both can be developed by CERN.

IV. CONCLUSION

The wideband kicker is the terminal element of the transverse feedback system being developed for the SPS. It is absolutely the critical element needed to realize intra-bunch feedback in the SPS. We have considered systems consisting of a stripline and two cavities, an array of four striplines, and a slotted-coaxial kicker. The slotted-coaxial kicker shows very promising characteristic

TABLE V. Summary of the number of feed throughs, loads, and power amplifiers and operating band necessary for each wideband kicker system.

System	Feed Throughs	Loads[a]	P_{amp} (W)	P_{total}	Band (MHz)
Stripline	4	2	500		DC − 400
Cavity	2[b]	1[b]	1000	3000	800(100)
Cavity	2[b]	1[b]	1000		1200(100)
Array of Four Striplines	16	8	500	4000	DC − 1000
Slotted-Coaxial Kicker	4	2	500	1000	DC − 1000
				OR	
			2000	4000	DC − 1000

[a] Each high power load requires monitoring and protection in case of loss of cooling.
[b] Each cavity requires at least one high power load/damper connected to a coupler port. Additional may be needed to get good coupling to all modes within the cavity.

consistent with the requirements for the system at high frequencies where as the array of striplines shows promise at low frequencies. In order to have a kicker built and installed by the end of LS1 with the performance specified, we recommend that both the array of striplines and the slotted-coaxial kicker undergo more detailed mechanical design and prototyping. After bench testing and vacuum testing we plan to see this structure installed in LSS3 in Sextant 3 of the SPS. Machine measurements with the wideband feedback demonstration system will follow shortly thereafter when the SPS resumes operations in 2014.

Appendix A: Transverse Cavity Kicker

1. Formalism

The cavity option is based on the assumption that the feedback system has a Gaussian frequency response with cutoff frequency, $\omega_c = 1$ GHz:

$$H(\omega) = H_0 e^{-\frac{\omega^2}{2\sigma_\omega^2}} \quad \text{(A1)}$$

The time resolution provided by the system is given by the inverse Fourier transform of its frequency response, which is still a Gaussian function with standard deviation $\sigma_t = 1/\sigma_\omega$:

$$v(t) = v_0 e^{-\frac{\sigma_\omega^2 t^2}{2}} \quad \text{(A2)}$$

The voltage kick can discriminate a portion of the bunch related to the waveform standard deviation σ_t. We can assume the waveform FWHM as the system intra-bunch time resolution capability τ_{res}:

$$\tau_{res} \approx FWHM = 2.35/\sigma_\omega \quad \text{(A3)}$$

For a 1 GHz bandwidth system, $\tau_{res} < 0.4$ ns. If we consider a sequence of Gaussian pulses with a repetition rate equal to the full bunch duration, τ_b, the effect on a given single bunch is expected to be the same:

$$v_p(t) = v_0 \sum_m e^{-\frac{\sigma_\omega^2 (t - m\tau_b)^2}{2}} \quad \text{(A4)}$$

The function $v_p(t)$ is clearly periodic with fundamental angular frequency $\omega_0 = 2\pi/\tau_b$ and can be expressed by a Fourier expansion:

$$v_p(t) = v_0 \sum_n a_n e^{jn\omega_0 t} \quad \text{(A5)}$$

with

$$a_n = \frac{1}{\tau_b} \int_{\frac{-\tau_b}{2}}^{\frac{\tau_b}{2}} v_p(t) e^{-jn\omega_0 t} \mathrm{d}t = a_0 e^{-\frac{n^2 \omega_0^2}{2\sigma_\omega^2}} \quad \text{(A6)}$$

The discrete spectrum has the same envelope as the continuous Gaussian one. If the feedback signal were really periodic, all of the bunches in the train would be affected. In order to kick only the bunch corresponding to $m = 0$, a damping term must be added to the periodic voltage, $v_p(t)$, with a decay time, τ_d, sufficiently shorter than the bunch separation, T_b, as shown in Fig. 10:

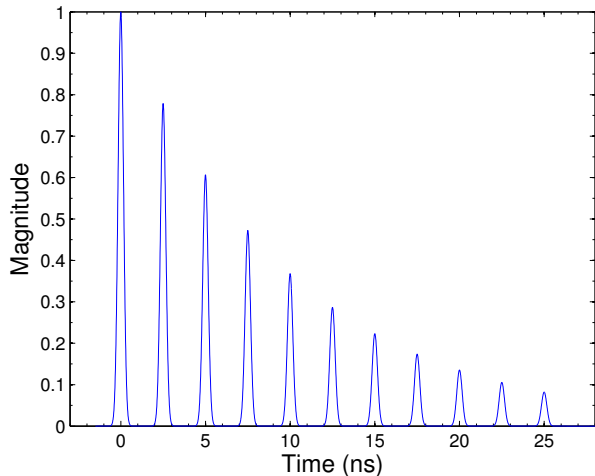$$V(t) = V_0 \sum_m e^{-\frac{\sigma_\omega^2 (t - m\tau_b)^2}{2}} e^{-\frac{t}{\tau_d}} \qquad \text{(A7)}$$

FIG. 10. A periodic voltage signal with a damping term confined by τ_d.

The Fourier transform gives the spectrum of the signal:

$$V_d(\omega) = V_0 \sum_n \frac{e^{-\frac{n^2 \omega_0^2}{2\sigma_\omega^2}}}{1 + j \frac{n \omega_0 \tau_d}{2} \left(\frac{\omega}{n\omega_0} - \frac{m\omega_0}{\omega} \right)} \qquad \text{(A8)}$$

which is simply a sequence of Lorentzian pulses confined by a Gaussian form factor as shown in Fig. 11. The reported frequency response has a much lower spectrum occupancy compared to the continuous one, but shows many resonances. For practical reasons one should limit a real system to a few of them. For instance, if we consider only the first three resonances, the response in the time domain is slightly deformed as shown in Fig. 12.

2. Cavity Design

The cavity design is a modified pill-box and the parameters of frequency, Q, and shunt impedance has been verified with simulations using HFSS [16]. The pillbox is coupled by rectangular waveguides through large apertures. Figure 13 shows a model of the proposed cavity. The input and output waveguides are coupled to a single
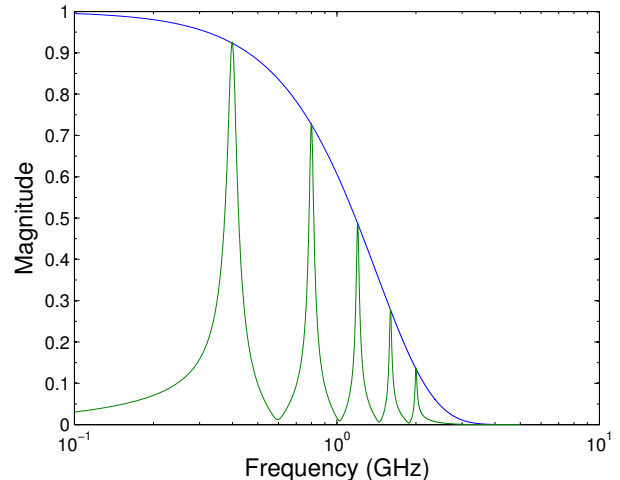
FIG. 11. Spectrum of five Lorentzian pulses representing kicks to a bunch of length, τ_b, with fundamental angular frequency ω_0. The pulses are confined by a Gaussian form factor shown in blue.
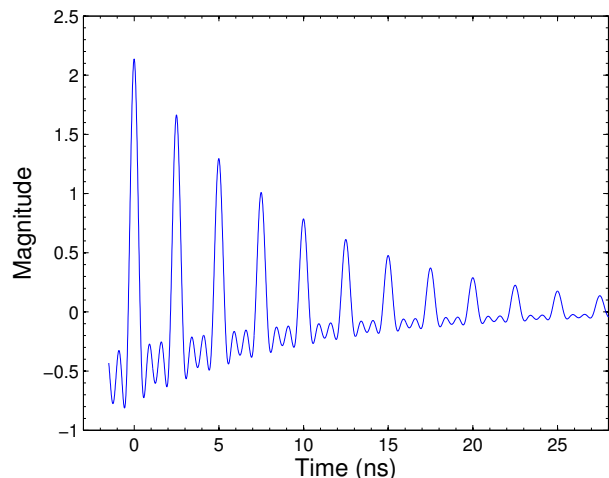

FIG. 12. The periodic voltage signal considering only the first three resonance. The voltage signal is slightly deformed.

cell cavity by two large, identical apertures. The beam pipe was modeled as a rectangle with rounded corners and dimensions 100 mm (H) × 36 mm (V), vertically, just under the stay-clear limit (see Sec. I C). Table VI shows the cavity parameters as simulated in HFSS.

The S_{21} parameter for the 800 MHz and 1200 MHz cavities is shown in Fig. 14. The 800 MHz cavity shows a bandwidth of 63 MHz and 57 MHz for the 1200 MHz cavity.
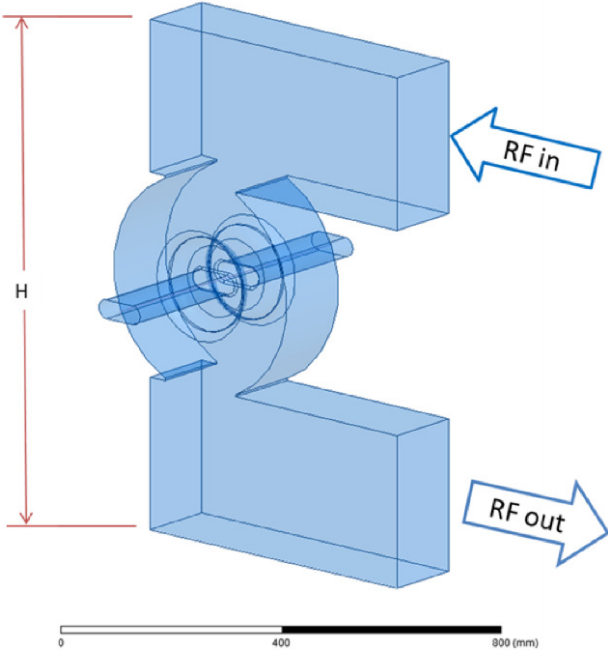
FIG. 13. Cavity design

TABLE VI. Transverse cavity parameters as simulated in HFSS.

Parameter	Cavity #1	Cavity #2
f (GHz)	0.8	1.2
Q	23	38
$R_\perp T^2$ (kΩ)	2.1	3.3
H (cm)	100	60
Beam pipe (mm^2)	100×36	100×36
WG standard	WR-1150	WR-650

Appendix B: Stripline Kicker

1. Stripline Design

Figure 15 shows a model of the tapered stripline geometry. The stripline electrodes are driven with oppo-
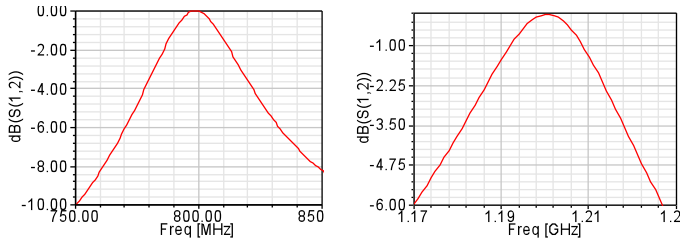
site voltages $\pm V_{\Delta/2}$ as 50 Ω transmission lines terminated on a matched load to provide transverse deflection to the beam. Shunt impedance and bandwidth of the system depend chiefly on the stripline length and we have chosen a value equal to 10 cm to optimize the response at 750 MHz. A longer stripline would give a larger shunt impedance at lower frequencies, but a smaller one at higher frequencies, and a shorter stripline would have the opposite characteristics, with a larger impedance at higher frequencies, but smaller at lower frequencies. In order to satisfy the stay-clear requirements the electrodes are separated by a vertical spacing of $h = 45$ mm and reside in a rectangular vacuum pipe with rounded corners of 130 mm (H) × 92.4 mm (V) as shown in Fig. 16. The stripline width is chosen equal to $w = 56$ mm to ensure the desired field homogeneity, as will be described in Sec. B 4.
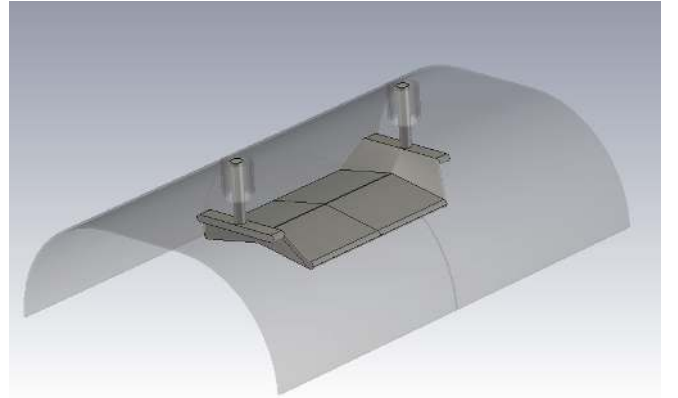
FIG. 15. Model of the stripline kicker design.

FIG. 14. S$_{21}$ parameters for the 800 and 1200 MHz cavities.
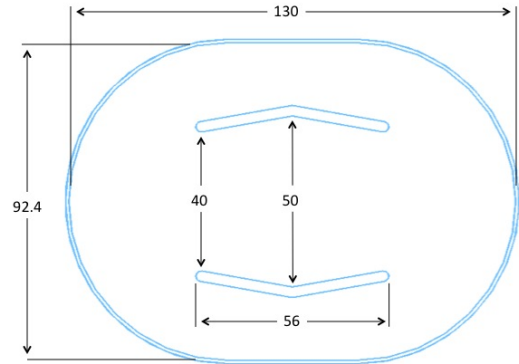

FIG. 16. 10 cm long stripline kicker dimensions.

2. Shunt Impedance

The transverse shunt impedance for a stripline can be analytically calculated via

$$R_\perp T_S^2 = 2Z_c \left(\frac{g_\perp L}{h/2}\right)^2 \left(\frac{\sin(kL)}{kL}\right)^2 \qquad \text{(B1)}$$

where Z_c is the characteristic impedance of the transmission line (50 Ω), $g_\perp \approx \tanh(\pi w/2h) \approx 0.95$ is the coverage factor of the stripline, L is the electrode length, and wave number, $k = \omega/\beta c$.

In order to evaluate how much the kicker's shunt impedance deviates from the ideal behavior described by Eq. B1, we have performed a virtual measurement of the component using the classic two-wire method [18] modeling the structure in CSTs Microwave Studio 3D electromagnetic analysis code [17]. Figure 17 shows the theoretical shunt impedance as calculated by Eq. B1 compared to the result based on the S_{21} parameter obtained from the simulation code according to the formula

$$R_\perp T_S^2 = \frac{2Z_{2w}}{k(\Delta x)^2} \left(\frac{S_{21}^{\text{ref}}}{S_{21}} - 1\right) \qquad \text{(B2)}$$

where Z_{2w} is the 2-wire impedance and Δx is the half-distance between the wire's electrical centers, as described in Ref. [19] and S_{21}^{ref} is the S_{21} parameter calculated for the same structure when the striplines are removed. Note that such a technique diverges at DC, due to the k-factor in the denominator of Eq. B2. The discrepancy between the theoretical and numerical values can be attributed in part to the large dimensions of the electrodes, which increase the stray capacitances, and therefore the electrode's electric length. Additionally, the tapering introduced to improve the impedance match between feed throughs and striplines at higher frequencies also contributes to the decrease in shunt impedance below the theoretical value.
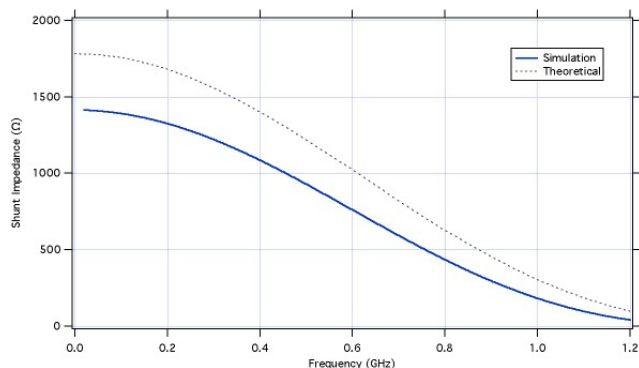

FIG. 17. Analytical and simulated shunt impedance values for the stripline kicker using the 2-wire virtural measurement. The simulation deviates from the theoretical because of the large dimensions of the strips.

The impedance matching of the stripline above 700 MHz has been improved by introducing some tapering, reducing the length of the in-vacuum part of the feedthroughs.

Table VII shows values of electrode voltages and peak and average power needed in the hypothesis of a single kicker module, using the theoretical value of the shunt impedance, calculated for the nominal transverse momentum kick 5×10^{-5} eV·s/m . Obviously, an array of stripline kickers needs to be used in order to reduce those figures to practical values. The electrode voltage is reduced linearly with the number of modules N_k and the power with its square. Therefore we estimate that, unless the transverse kick necessary above 750 MHz is revised downward, a minimum of 16 modules would be necessary using 500 W amplifiers.

3. Coupling Between Multiple Kicker Modules

Crosstalk between adjacent modules can be evaluated by calculating the attenuation of a 1 GHz signal generated by one module across the length of vacuum chamber that separates it from the next module. For lower frequencies this attenuation will be larger.

If the beampipe cutoff is $f_{co} \approx 1.3$ GHz, the attenuation length $k_z \approx 17$ m^{-1} can be easily calculated from

$$k_z = \frac{2\pi}{c}\sqrt{f_{co}^2 - f^2}. \qquad \text{(B3)}$$

The minimum separation distance if we want to use four modules is 15 – 20 cm, in order to house them in a 1 meter long section, which is the length likely available for kicker installation. For such a separation the field from one module will be attenuated by at least 20 dB before reaching the next one.

4. Field Homogeneity

Given the beam transverse dimensions at the kicker location and the horizontal drift during the ramp, we defined a suitable region of homogeneity for the deflecting field of about ±15 mm (H) × ±10 mm (V), the horizontal requirement being the more stringent one. We designed a 56 mm wide stripline with hedges shaped to improve the field quality and obtained a uniformity better than 2% over a 25 mm wide region as shown in Fig. 18.

5. Beam Coupling Impedance

We analyzed the longitudinal coupling impedance of the proposed stripline kicker using a procedure similar to the one mentioned above for the shunt impedance: A well known bench test method, this time with a single coaxial wire, has been implemented on Microwave Studio obtaining a virtual measurement of the coupling impedance

TABLE VII. Voltage and power estimates per electrode of a single stripline kicker of 10 cm length. Note, values computed here using the theoretic shunt impedance and nominal momentum change of 5×10^{-5} eV·s/m.

Frequency (MHz)	Electrode Voltage (V)	Shunt Impedance (Ω)	P_{max} (kW)	$P_{avg.}$ (kW)
DC	1780	1780	31.5	6.3
250	1860	1630	34.6	6.9
500	2150	1220	46.1	9.2
750	2800	720	78.5	15.7
1000	4300	305	185	37.0
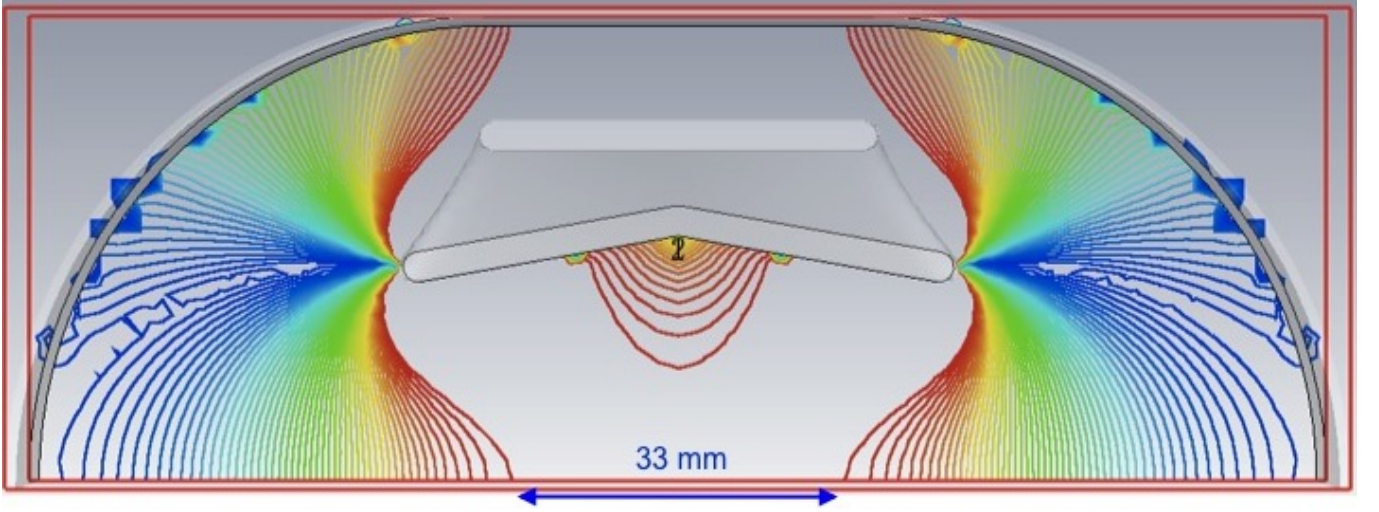
FIG. 18. Transverse electric field homogeneity. The isolines are spaced by 2% changes of the value of the deflecting field.

using the formula

$$Z_{||} = 2Z_w \left(\frac{S_{21}^{ref}}{S_{21}} - 1 \right) \tag{B4}$$

where Z_w is the coaxial line impedance. In the result shown in Fig. 19 one can notice how the component deviates from the theoretical result expected for an ideal structure as the frequency approaches 1 GHz, again mostly due to the TE_{01} mode propagation. The first maximum is nonetheless at 750 MHz, as expected. Considering that the LHC bunch have a $\sigma_z = 0.7$ ns, we can easily derive an estimate for the longitudinal loss factor as

$$\kappa_{||} < \frac{2}{\pi\sigma_z} 40\Omega \approx 0.04 V/pC \tag{B5}$$

which is but a negligible value, even considering the use of several kicker modules, from the point of view of beam dynamics being equivalent to a loss in the 1 keV range, which has to be compared to the 26 GeV minimum SPS energy. Considering the power deposited on the kicker from the fully loaded SPS (e.g., 4 batches of 72 bunches at 1.15×10^{11} p/bunch) beam, we obtain a value around 250 W, which will be split by the two striplines of each module. This is a rather substantial value, which requires

protecting the amplifier from beam induced voltage and ensuring good impedance matching on the other stripline feed through.
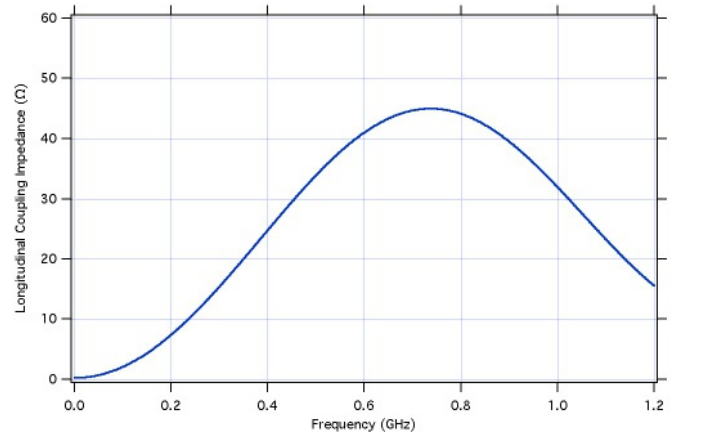

FIG. 19. Longitudinal beam coupling impedance for a 10 cm long stripline kicker module as evaluated by a virtual coaxial wire measurement.

Appendix C: Slotted Kicker

The slotted kicker geometries evaluated in this study are similar to those used for stochastic cooling in Refs. [4] and [5]. The dimensions of the structures can be tuned in such a way as to yield the necessary bandwidth. The slotted-waveguide kicker consists of a waveguide coupled to a beam pipe via slots and is most similar to that of Ref. [5]. The low frequency cutoff of the structure is determined by the width (broad dimension) of the waveguide. The larger the dimension, the lower the frequency reach. The slotted-ridged waveguide is an extension of the slotted-waveguide kicker, with a ridge incorporated into the waveguide to concentrate the field in the ridge region. The slotted-coaxial kicker resembles that of Ref. [4], a so-called Faltin-type slotted kicker, containing a coaxial transmission line within the waveguide. Because of the coaxial line, this structure has virtually no lower cutoff frequency. Figure 20 shows quarter models of the three slotted kickers explored in this study. These structures were evaluated initially as conceptual models, i.e., without detailed power coupling ports or dielectric materials in order to estimate the usefulness of such structures. Since the kicker will be located in a region near the MBB dipole magnets, the simulated beam pipe dimensions matched exactly those of the MBB dipoles, 132 mm × 52.3 mm, to absolutely comply with the stay clear limits. In principle, if more kick strength is needed the vertical dimensions can be reduced by ∼20% to 45 mm. Initially, the goal was to maximize the shunt impedance over a bandwidth of 1 GHz for each of the three structures, comparing each. Table VIII lists the initial parameters used in the simulations for each structure and Fig. 21 shows an end view of the slotted-coaxial kicker with dimensions listed. For reference, in the HFSS simulations, vertical is defined in the x-direction and horizontal in the y-direction. The beam axis is along the z-direction.

1. Transverse Shunt Impedance

The structures were modeled and the fields were produced by modal excitations at frequencies in the operating band. Upon integrating the fields along the beam trajectory via Eq. 4, $V_\perp$ can be computed and subsequently $R_\perp T^2$ via Eq. 3 for a constant input power. Quarter geometries were modeled to save on computation time by utilizing symmetry. Perfect magnetic boundary conditions were applied for the xz-plane and perfect electric boundary conditions for the yz-plane to simulate the vertical kick.

Figure 22 shows the transverse shunt impedance calculated with parameters listed in Tab. VIII for the three slotted kickers. The slotted-waveguide kicker exhibits the most narrowband response with a peak in shunt impedance of 58 kΩ at about 950 MHz. The FWHM bandwidth of this structure is 150 MHz. Introducing a ridge into the waveguide increases the bandwidth to 300
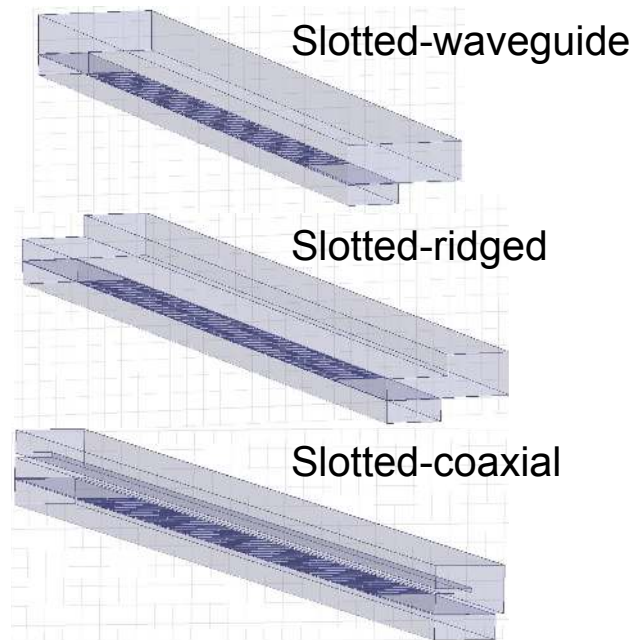

FIG. 20. Quarter model geometries of the three slotted type kickers evaluated in this study.
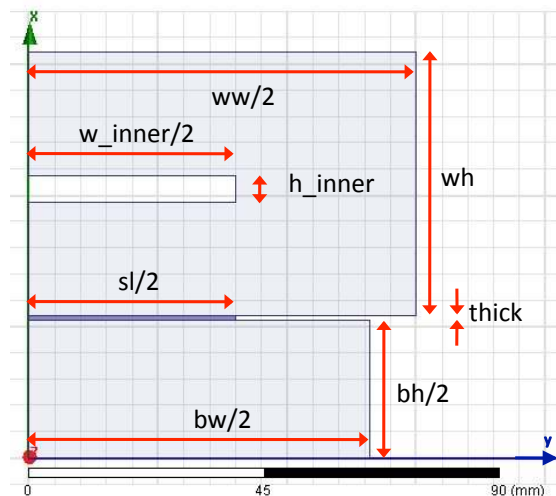

FIG. 21. End view (xy-plane) of a quarter model of the slotted-coaxial kicker with dimension parameters listed. Additional parameters in the z-direction include the slot width (sw), slot spacing (ss), length of the slotted section (al). The beam axis is along the z-direction.

MHz and shifts the operating point to lower frequency, peaking at 780 MHz with a shunt impedance of 27 kΩ. The slotted-coaxial kicker is extremely wideband, spanning from nearly DC to greater than 1200 MHz for the 80 mm slot length case. The frequency response varies greatly by changing a single parameter, the slot length. We show in Fig. 22 for two cases, at 125 mm where the

TABLE VIII. List of the initial parameters of the slotted-waveguide (WG), slotted-ridged (Ridge), and slotted-coaxial (Coaxial) kickers. These parameters correspond to those used to calculate the transverse shunt impedance shown in Fig. 22 and phase of the voltage shown in Fig. 23.

Parameter	Description	Direction	Lengths (mm)		
			WG	Ridge	Coaxial
al	Length of slotted section	z	1000	1000	1000
bh	Beam pipe height	x	52.3	52.3	52.3
bw	Beam pipe width	y	132	132	132
thick	Slot interface thickness	x	1	1	1
wh	Waveguide height	x	50	50	50
ww	Waveguide width	y	300	300	150
ss	Slot spacing	z	20	20	20
sl	Slot length	y	125	125	125 & 80
sw	Slot width	z	5	5	5
L	Length of vacuum pipe at ends	z	200	200	200
h_ridge	Ridge height	x	-	25	-
w_ridge	Ridge width	y	-	150	-
h_inner	Coaxial line thickness	x	-	-	5
w_inner	Coaxial line width	y	-	-	80

response rolls off at 800 MHz and at 80 mm where the response rolls off at 1200 MHz. The shunt impedance of the 80 mm slot length case is nearly half at 4 kΩ than that of the 125 mm case. This simple comparison illustrates how a single parameter can drastically change the frequency response and magnitude of the shunt impedance.
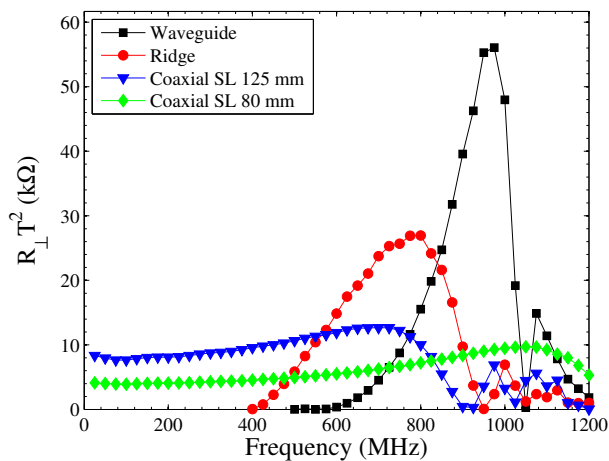

FIG. 22. Transverse shunt impedance calculations for the three variations of the slotted kicker. The parameters used for the calculation are listed in Tab. VIII. The slotted-coaxial kicker shunt impedance is plotted for two different slot lengths (sl).

The phase of the transverse voltage generated by the structure, $V_\perp$, must be understood since it has implications for the overall transfer function of the feedback system. Ideally, one would like the phase to be constant or smoothly varying. Figure 23 shows the transverse phase of the voltage on axis, $\phi_{V_\perp}$, with respect to frequency for the three slotted kickers. The slotted-coaxial kicker has linear phase response at low frequencies. In comparing Fig. 22 to Fig. 23, the phase becomes irregular at frequencies only where the shunt impedance peaks. The phase is irregular for the entire operating band of the slotted-waveguide and -ridged kickers. Equalizing such a phase response could be extremely difficult and must be considered for implementation.
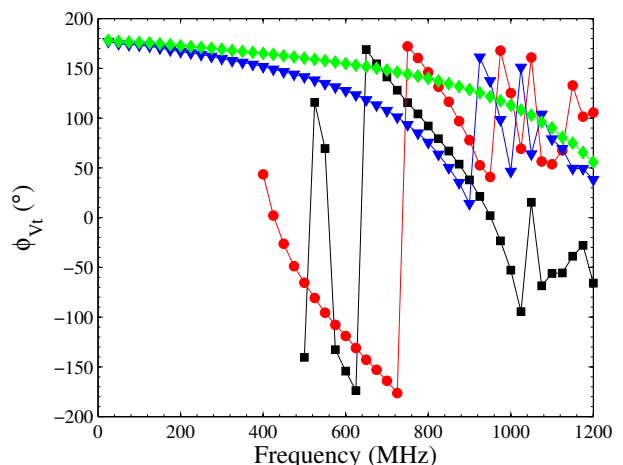

FIG. 23. Phase of the transverse voltage. Color and symbol coding is the same as in Fig. 22.

When finding the transverse shunt impedance, $V_\perp$ must be determined by integrating the fields via Eq. 4. In evaluating this structure, it is important to understand which field dominates the integral for $V_\perp$. Figure 24 shows the total transverse shunt impedance (in black), the shunt impedance from the electric field component (in red), and from the magnetic field component (in blue).

At low frequencies, the kick arises largely from the transverse magnetic field. It is not until 600 MHz, that the electric field begins to contribute to the kick. Figure 24 represents the shunt impedance computed for the parameters listed in Tab. III, the final optimized structure. The results from the optimization of parameters are presented in Sec. C 2.
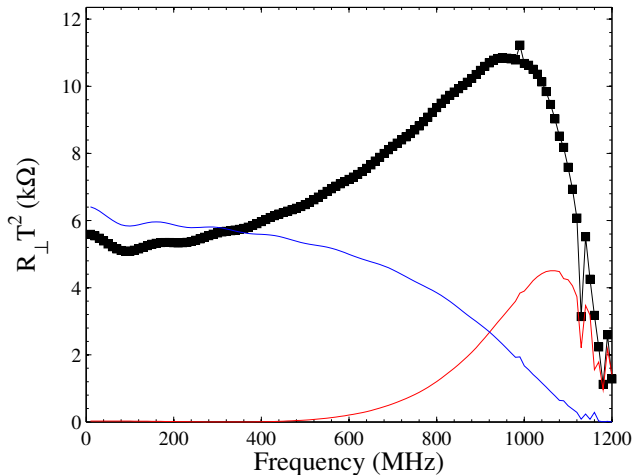

FIG. 24. Transverse shunt impedance curves of the slotted-coaxial structure with contribution from both the electric and magnetic fields (black), and each field separately, electric (red) and magnetic (blue). The black curve represent the shunt impedance calculated for the parameters listed in Tab. III.

2. Optimizing the Slotted-Coaxial Kicker

The slotted-coaxial kicker appears to be a very attractive option because of its wideband coverage, shunt impedance magnitudes (rivaling those of the stripline and cavity kickers), and its smoothly varying phase. Further studies scanning the geometrical parameter space to optimize the bandwidth and shunt impedance were performed for the slotted-coaxial structure. The dimensions of the entire slotted-coaxial kicker were parameterized for optimization, maximizing the shunt impedance as well as bandwidth of the kicker. We present the results of parameter scans that most influence these two criteria.

a. Slot Periodicity

For a constant 25 mm slot width-spacing pair distance (ss+sw, along the beam axis, z), a fixed number of 40 slots over 1 m length, and a slot length of 80 mm, dimensions of the a slot width were varied. An optimal slot width to spacing aspect ratio was about 1 to 1 (when w = ss = 12.5 mm), which maximizes the shunt impedance over the frequency range. Figure 25 shows the transverse

shunt impedance for the slot widths listed in the legend. The frequency response is minimally affected, with just a slight shift in the peak to lower frequency when the slot width to spacing ratio is nearly equal.
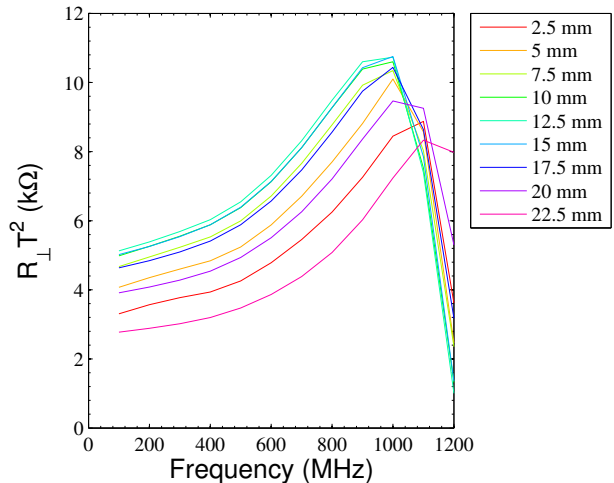

FIG. 25. Transverse shunt impedance curves of the slotted-coaxial structure when varying the slot width, keeping the slot width-spacing pair 25 mm, the number of slot totaling 40 in 1 m, and a slot length of 80 mm. The maximum shunt impedance over the frequency range desired occurs when the slot width is 12.5 mm, or when the width to spacing ratio is 1 to 1.

b. Number of Slots in 1 m

The number of slots within 1 m were varied. For example, reducing the slot width-spacing pair distance from 25 mm to 12.5 mm doubles the number of slots (80) that can fit into the 1 m length. Likewise, for a slot width-spacing pair distance of 50 mm, the number slots in 1 m is cut in half to 20. Figure 26 shows the transverse shunt impedance for these two situations. When the number of slots is doubled to 80, there is an increase in the shunt impedance by about 25%. For 20 slots, the shunt impedance is reduced by 35%. The frequency response is minimally affected, with just a slight shift in the peak to lower frequency for the increased number of slots. If more kick is needed, increasing the number of slots could be a method to increase the shunt impedance further (at the expense of increased beam coupling impedance).

c. Length of Kicker

The length of the slotted kicker was varied from 10 cm to 200 cm for a constant slot width-spacing pair distance of 25 mm. Thus, a 10 cm long structure has 4 slots and a 200 cm structure has 80 slots. Figure 27 shows
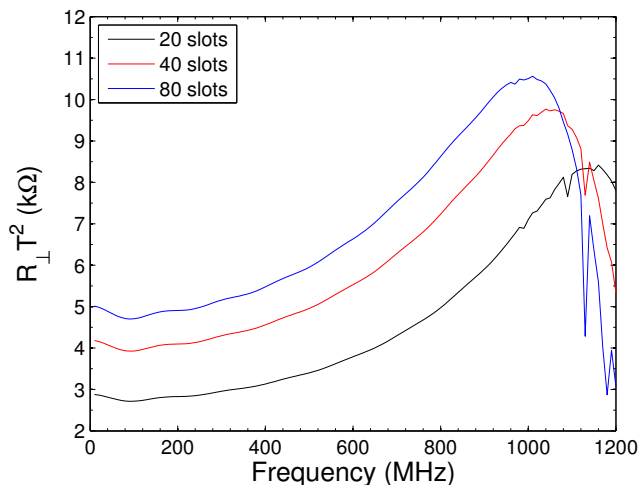
FIG. 26. Transverse shunt impedance curves of the slotted-coaxial structure when doubling (80) and halving the number of slots (20) in 1 m. Note, the slot width to spacing ratio for these simulations was 1 to 4 with slot length 80 mm.

the transverse shunt impedance for the lengths listed in the legend. The frequency response is reduced when the structure is longer, but the shunt impedance is dramatically increased. For instance, when doubling the length of the slotted kicker to 200 cm and thus the number of slots, the shunt impedance is increased by a factor of 4 but the frequency begins to roll off at 800 MHz. When the length is halved, the shunt impedance decreases by a factor of 4, but the frequency response is increased.
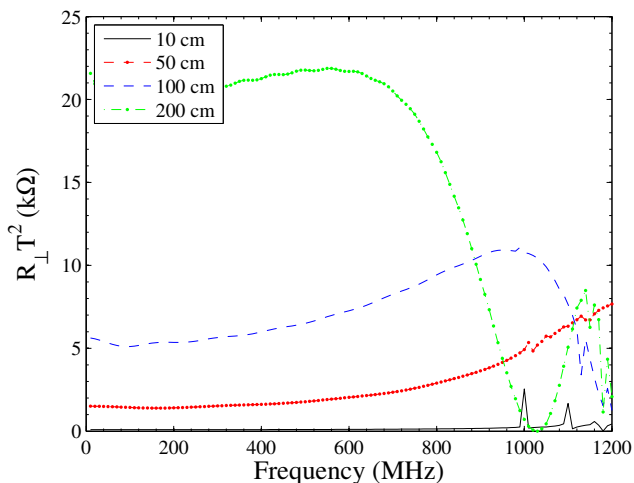
FIG. 27. Transverse shunt impedance curves of the slotted-coaxial structure where the length of the slotted structure (al) is varied, but the slot width-spacing distance is fixed at 25 mm. Note, slot width to spacing ratio for these simulations was 1 to 1.

d. Slot Length

The slot length (sl) was varied from 50 mm to 120 mm and was found to have large influence on the shunt impedance and frequency response. For small slot length the shunt impedance is smallest over the operating band. However, as the slot length increases, the operating band decreases. For instance, with a slot length of 50 mm, there is nearly constant shunt impedance of 1 kΩ over the 1 GHz band, while for the 120 mm case, the shunt impedance gradually increases from 7 – 12 kΩ over 100 – 700 MHz, then falls quickly there after. While the goal is to maximize the shunt impedance over the 1 GHz operating band, a good compromise seems to be with a slot length of 80 mm, and is considered the optimum value. The shunt impedance gradually increases from 4 – 9 kΩ over 100 – 1000 MHz, the band of interest.
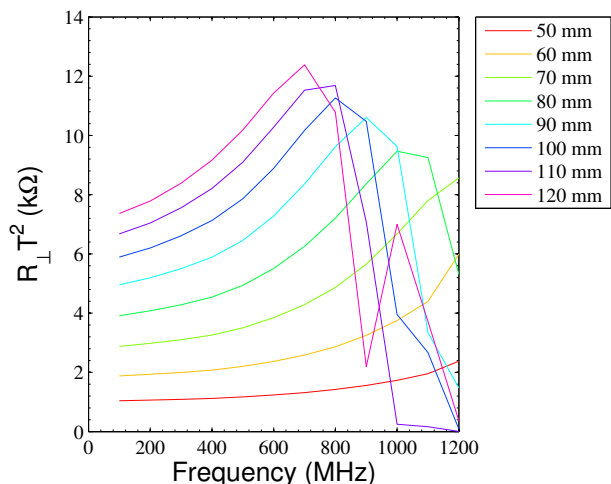

FIG. 28. Transverse shunt impedance curves of the slotted-coaxial structure when varying the slot length, sl. Note, the slot width to spacing ratio for these simulations was 1:4.

3. Transverse Uniformity

In order to cover a bandwidth up to 1 GHz, with reasonable shunt impedance, a slot length of 80 mm was chosen to investigate the transverse uniformity of the voltage kick on axis. Unlike the stripline case, we cannot just look at the uniformity of the electric field since the kick contribution is magnetic at low frequencies and electric at high frequencies. In order to look at the transverse uniformity of the slotted-coaxial kicker, we look at the consistency of the shunt impedance when the beam is assumed off axis (i.e., when the fields are integrated off axis). Figure 29 shows the transverse shunt impedance when the beam is horizontally displaced off axis (fields are integrated in 5 mm steps horizontally) and a slot

length of 80 mm. As the beam moves horizontally from the beam axis, the kick strength decreases. At 20 mm off axis, the shunt impedance is reduced by 39%. Recall that $R_\perp T^2 \sim V_\perp^2$, which means that the transverse voltage on axis is actually down by 62%. Simulations were repeated for a slot length of 125 mm. At 20 mm off axis, the shunt impedance is reduced by 18%. These are not negligible reductions and must be taken into consideration for operation. The vertical uniformity of the shunt impedance was investigated with similar simulations. The shunt impedance when the beam is located vertically 15 mm off axis is slightly larger by about 10% as compared to the on axis case, but has less of an importance compared to the horizontal uniformity.
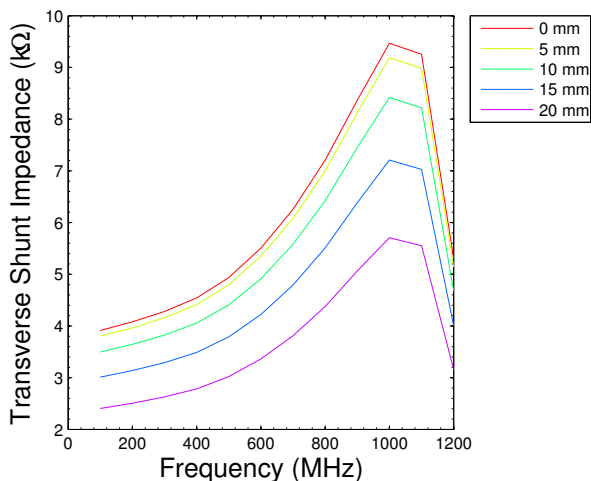

FIG. 29. Transverse shunt impedance curves of the slotted-coaxial structure when the beam is displaced horizontally (y-direction) off axis. The slotted parameters for this simulations: sl = 80 mm, sw = 5 mm, ss = 20 mm.

The transverse shunt impedance at a transverse point x = 15 mm, y = 20 mm was simulated and compared to the case on axis. Figure 30 shows the transverse shunt impedance comparing the two cases. The shunt impedance at the transverse location is decreased by <10% of that on axis.

4. Beam Coupling Impedance

In order to evaluate the contribution of the slotted-coaxial kicker into the overall SPS impedance budget, we have carried out numerical simulations with GdfidL [15]. The dimensions used for these calculations are in Tab. III. We found that for the perfectly matched coaxial waveguides, both longitudinal and transverse impedances remain essentially broadband (without very narrow HOM-like peaks) until rather high frequencies ∼5 GHz. The beam length used for these simulations was σ_z = 2 cm. Figure 31 shows the longitudinal wake potential with a
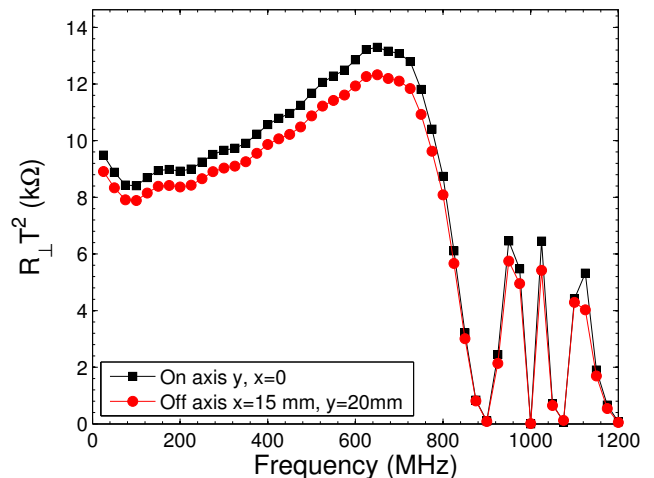

FIG. 30. Transverse shunt impedance curves of the slotted-coaxial structure on axis (black) and when the beam is displaced at point vertically, x = 15 mm and horizontally, y = 20 mm (in red). Note, the slot length for these simulations was 125 mm.

σ_z = 2 cm Gaussian distribution. The resulting wake fields decay very fast. The wakes almost disappear before the arrival of successive bunches (red vertical line corresponding to 25 ns bunch spacing). This helps in avoiding harmful multibunch effects such as conventional multibunch instabilities and a power loss enhancement due to interaction with higher-order modes.
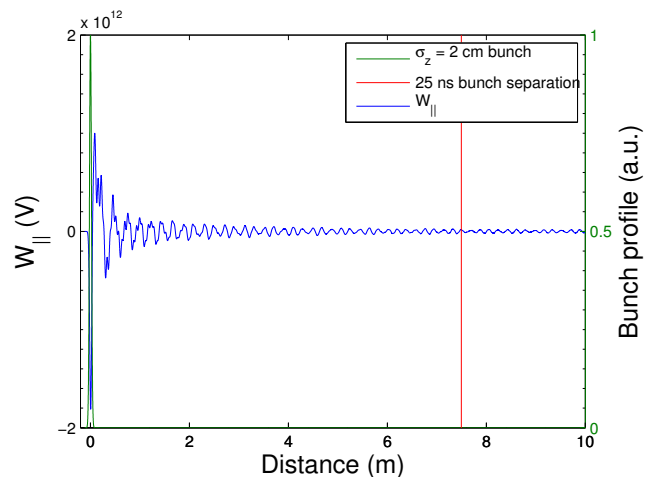

FIG. 31. Longitudinal wake potential generated by passing a 2 cm long bunch through the 1 m long slotted structure. The red vertical line marks the arrival of the next successive bunch in a typical 25 ns filling pattern and demonstrates that the wake fields at that point are negligible.

Figure 32 shows the Fourier transform of the wake potential normalized to the bunch spectrum, the longitudi-

nal impedance, $Z_{||}$, both real and imaginary components. From the real part of the longitudinal impedance and beam spectral power density, we can calculate the loss factor of the beam when passing through the structure via

$$\kappa_{||} = \frac{1}{\pi} \int_0^\infty \text{Re}[Z_{||}]\lambda(\omega)^2 d\omega \qquad (C1)$$

where

$$\lambda(\omega) = \exp\left[\frac{-\omega^2\sigma_z^2}{2c^2}\right] \qquad (C2)$$

the density of a Gaussian distribution. If we take $\sigma_z = 20$ cm (0.7 ns bunch length at injection), the loss factor amounts to $\kappa_{||} = 0.006$ V/pC. As a worst case scenario, if we take the bunch length at flat top to be 0.35 ns, the loss factor is 0.04 V/pC, which corresponds to an energy change in the 450 GeV beam of >1 keV. Neglecting the coupling between bunches, for a fully loaded beam in the SPS (4 batches of 72 bunches, 1.5×10^{11} p/bunch), this corresponds to a beam power of 250 W, which will be split between two waveguides. The directivity of this power has only been initially explored, and it appears that most power transfers to the downstream ports, not the upstream ports, where the power amplifiers are located. Results are forthcoming on the power directivity.
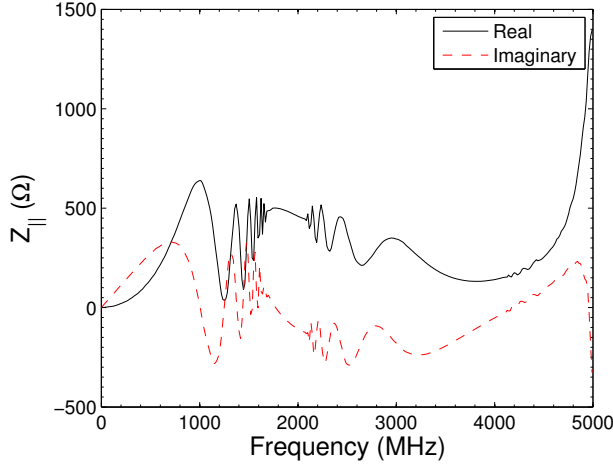

FIG. 32. Real and imaginary parts of the longitudinal beam coupling impedance for the slotted structure.

The transverse (vertical) wake potential has also been computed and is shown in Fig. 33. Again, a 2 cm long bunch was simulated, but with a vertical displacement from axis of 2 mm. The wake fields decay very rapidly and are virtually nonexistent by the time the next bunch arrives.

The transverse impedance is shown in Fig. 34, for both real and imaginary components. The broadband kicker impedance is expected to be a small fraction of the total SPS impedance. For example, the estimated transverse broadband impedance is less than 100 kΩ/m, to be
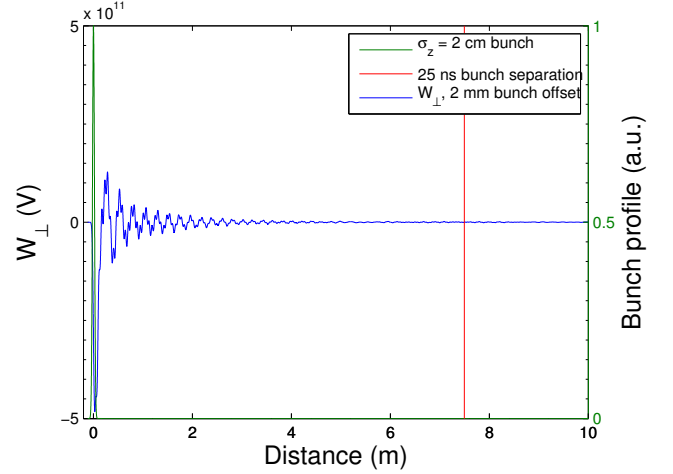

FIG. 33. The transverse wake potential from a 2 cm long bunch. The red line marks the 25 ns bunch separation.

compared with 7 MΩ/m, which is the contribution of all other installed SPS kickers. The impedance is also <1% of the total SPS transverse impedance of 18 MΩ/m. The kick factor of this structure can be computed in a similar fashion as the loss factor, using the imaginary part of the transverse impedance via

$$\kappa_\perp = \frac{1}{\pi} \int_0^\infty \text{Im}[Z_\perp]\lambda(\omega)^2 d\omega. \qquad (C3)$$

For a bunch at injection, kick factor is 30.4 V/pC/m and at flat top the kick factor is 57.8 V/pC/m.
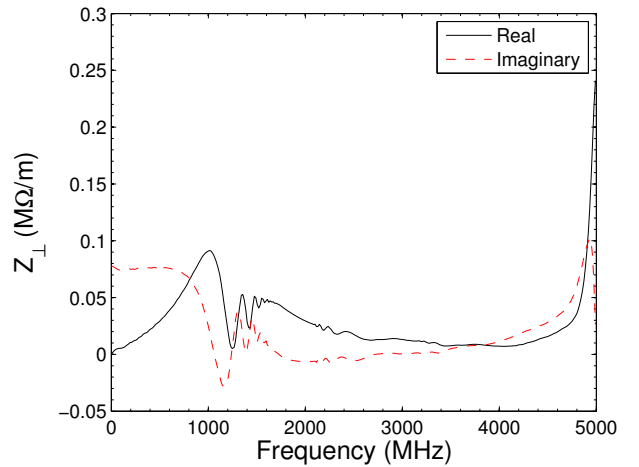

FIG. 34. Real and imaginary parts of the transverse beam coupling impedance for the slotted structure.

5. Port Design and Matching

The results presented until now have all been for an idealized slotted structure case. Power couplers have not been included in the simulation. This section presents the initial results on port design and development for the slotted-coaxial structure. The power enters the in upstream portion of the structure by coaxial lines in the x-direction matched closely to 50 Ω. The coaxial line intercepts the stripline. This interface is a very sensitive and can cause reflections, so the ends of coaxial lines are tapered to the stripline to help with matching the interface. The stripline itself was simulated to have steps in the $y-$ and $z-$directions tapering to the coaxial line to help minimize reflections. A step in the waveguide below the stripline was also included to help in matching.
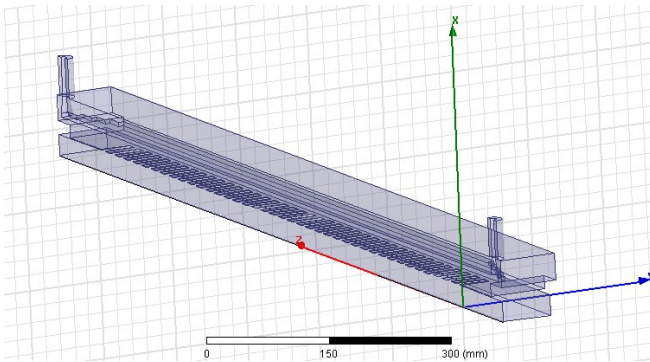

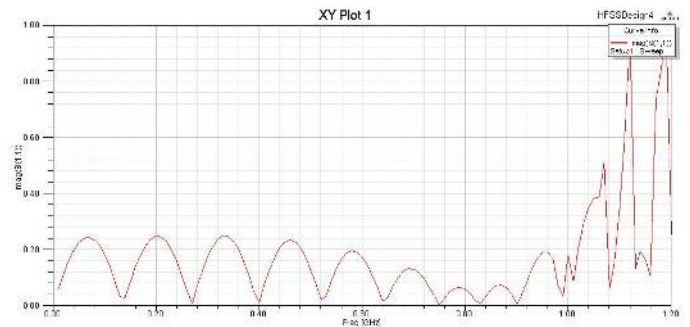FIG. 35. The coaxial to stripline power coupler interface.

FIG. 36. S_{11} parameter for the slotted-coaxial kicker as modeled with power coupling ports.

The process of matching took place in several design iterations by breaking the structure down into pieces. The coaxial to stripline interface was evaluated initially, where a stripline was contained within a waveguide without any slots. The S_{11} parameter was minimized by varying the parameters of the simulation. Next, a short region of the slotted section was added to the coaxial to stripline interface. Again, the parameters were varied to minimize S_{11}. Finally, a complete scale design with an identical input and output port was simulated and the model is shown in Fig. 35. The ports were defiined at the entrance of the coaxial lines. The S_{11} parameter for the initial simulation is shown in Fig. 36. There is a periodic behavior in the S_{11} parameter with frequency about 130 MHz. This corresponds to reflections between the two ports. This model has not yet been optimized and is currently being further refined. However, it shows that matching such a structure is indeed possible. These simulations does not contain any dielectric material, which would also need to be added for a more realistic S_{11} parameter.

[1] O. S. Brüning and F. Zimmerman, Proc. of IPAC 2012 **MOPPC005**, 127 (2012).
[2] B. Goddard *et al.*, Proc. of IPAC 2013 **WEPEA053**, 2624 (2013).
[3] R. Garoby *et al.*, Proc. of IPAC 2013 **THPWO077**, 3936 (2013).
[4] L. Faltin, Nucl. Instrum. Methods **148**, 449 (1978).
[5] D. McGinnis, IEEE Part. Acc. Conf. **1**, 59 (1999).
[6] P. Collier *et al.*, *The SPS as InJector for LHC Conceptual Design*, Tech. Rep. CERN-SL-97-07 DI (CERN, 1997).
[7] G. Iadarola, H. Bartosik, M. Driss Mensi, H. Neupert, and M. Rumolo, G. and Taborelli, IPAC'13 **WEPEA014**, 2525 (2013).
[8] G. Rumolo, *Applications of the SPS High Bandwidth Transverse Feedback System and Beam Parameters*, Tech. Rep. (2013).
[9] M. Benedikt, P. Collier, V. Mertens, J. Poole, and K. Schindl, *LHC Design Report Vol. 3*, Tech. Rep. (Geneva, 2004).
[10] B. W. Zotter, *The effective coupling impedance for bunched beam instabilities*, Tech. Rep. CERN-ISR-TH-78-16 (CERN, 1978).
[11] C. Zannini, *Electromagnetic Simulation of CERN Accelerator Components and Experimental Applications*, Ph.D. thesis, Ecole Polytechnique Federale de Lausanne (2013).
[12] T. P. R. Linnecar, IEEE Trans. Nucl. Sci. **26**, 3409 (1979).
[13] D. A. Goldberg and G. R. Lambertson, AIP Conf. Proc. **249**, 539 (1992).
[14] K. Kwok, A. Candel, L. Ge, A. Kabel, R. Lee, Z. Li, C. Ng, V. Rawat, G. Schussman, and L. Xiao, *Advances in Parallel Electromagnetic Codes for Accelerator Science and Development*, Tech. Rep. SLAC-PUB-14349 (SLAC).
[15] http://www.gdfidl.de.
[16] http://www.ansys.com.

[17] http://www.cst.com.

[18] G. Lambertson and D. Goldberg, CBP-Tech Note **122**.

[19] J. Corlett, Proc. of EPAC 1994 (1994).